Dynamics in *Thermotoga neapolitana* Adenylate Kinase: ^{15}N Relaxation and Hydrogen−Deuterium Exchange Studies of a Hyperthermophilic Enzyme Highly Active at 30 °C[†]

Harini Krishnamurthy,[‡,§] Kim Munro,[||] Honggao Yan,[⊥] and Claire Vieille*[,⊥,#]

Program in Cell and Molecular Biology, Michigan State University, East Lansing, Michigan 48824, Queen's Protein Function Discovery Facility, Queen's University, Kingston, Ontario, Canada K7L-3N6, and Department of Biochemistry and Molecular Biology and Department of Microbiology and Molecular Genetics, Michigan State University, East Lansing, Michigan 48824

Received October 27, 2008; Revised Manuscript Received January 16, 2009

ABSTRACT: Backbone conformational dynamics of *Thermotoga neapolitana* adenylate kinase in the free form (TNAK) and inhibitor-bound form (TNAK*Ap5A) were investigated at 30 °C using ^{15}N NMR relaxation measurements and NMR monitored hydrogen−deuterium exchange. With kinetic parameters identical to those of *Escherichia coli* AK (ECAK) at 30 °C, TNAK is a unique hyperthermophilic enzyme. These catalytic properties make TNAK an interesting and novel model to study the interplay between protein rigidity, stability, and activity. Comparison of fast time scale dynamics (picosecond to nanosecond) in the open and closed states of TNAK and ECAK at 30 °C reveals a uniformly higher rigidity across all domains of TNAK. Within this framework of a rigid TNAK structure, several residues located in the AMP-binding domain and in the core−lid hinge regions display high picosecond to nanosecond time scale flexibility. Together with the recent comparison of ECAK dynamics with those of hyperthermophilic *Aquifex aeolicus* AK (AAAK), our results provide strong evidence for the role of picosecond to nanosecond time scale fluctuations in both stability and activity. In the slow time scales, TNAK's increased rigidity is not uniform but localized in the AMP-binding and lid domains. The core domain amides of ECAK and TNAK in the open and closed states show comparable protection against exchange. Significantly, the hinges framing the lid domain show similar exchange data in ECAK and TNAK open and closed forms. Our NMR relaxation and hydrogen−deuterium exchange studies therefore suggest that TNAK maintains high activity at 30 °C by localizing flexibility to the hinge regions that are key to facilitating conformational changes.

Hyperthermophilic archaea and bacteria thrive at temperatures above 80 °C, and their enzymes have unique structure−function properties of high stability and optimal activity at high temperatures. Hyperthermophilic proteins have been intensively studied for over 30 years to understand the molecular determinants and physical principles underlying protein thermostability and because thermostable enzymes have potential biotechnological applications (see ref *1* for a comprehensive review).

Many hyperthermophilic enzymes are optimally active above 80 °C, and they are mostly inactive at low temperatures (i.e., around 20−37 °C) (*2*−*4*). The catalytic rates of homologous mesophilic, thermophilic, and hyperthermophilic enzymes are usually comparable at the respective optimal growth temperatures of their source organisms (*5*). These properties of hyperthermophilic proteins have been explained by invoking the role of protein dynamics in catalysis. The reduced activity of hyperthermophilic enzymes at low temperatures appears to support the hypothesis that hyperthermophilic proteins are more rigid than their mesophilic homologues at ambient temperatures. It is thought that enzyme motions required for activity become too slow and too restrained in hyperthermophilic enzymes at low temperatures and that these proteins gain the flexibility required for optimal activity only at higher temperatures. Lack of activity at low temperatures need not be a consequence of stability at high temperatures, though, as shown by a number of laboratory-evolved thermostable enzymes that are catalytically efficient at low temperatures (*6*). Also, as pointed out by Lazaridis et al. (*7*), an increase in flexibility should in fact contribute to the thermodynamic stability of the folded state through an increase in entropy. Understanding the role of protein dynamics in stability and activity requires appreciation of the fact that the protein energy landscape includes small fluctuations around the native state as well as transitions between conformational substates, including local and global unfolding events. These dynamic processes are spread across various time scales ranging from picosec-

[†] H.K. was supported in part by a fellowship from the Michigan State University Center for Biological Modeling.

* Corresponding author. Tel: (517) 884-5392. Fax: (517) 353-8957. E-mail: vieille@msu.edu.

[‡] Program in Cell and Molecular Biology, Michigan State University.

[§] Current address: Vollum Institute, Oregon Health and Science University, Portland, OR 97239.

[||] Queen's Protein Function Discovery Facility, Queen's University.

[⊥] Department of Biochemistry and Molecular Biology, Michigan State University.

[#] Department of Microbiology and Molecular Genetics, Michigan State University.

10.1021/bi802001w CCC: $40.75
Published on Web 02/16/2009

FIGURE 1: Alignment of TNAK, ECAK, and AAAK sequences using ClustalW. Helices (bars) and β-strands (arrows) based on the ECAK and AAAK crystal structures and TNAK 3D model are indicated above the sequence.

onds to milliseconds or slower. Dynamics on slower time scales involve transitions to substates that are separated by an energy barrier. Passage from the folded state to an unfolded state and vice versa is therefore characterized by large amplitude collective motions occurring on a time scale of milliseconds or slower. Since the increase in the free energy of stabilization for a hyperthermophilic protein is similar to that of a mesophilic protein, the stability of hyperthermophilic proteins may be due to a higher kinetic barrier separating the folded and unfolded states. Recent studies have suggested that such rare large amplitude conformational events may be assisted by more frequent small-amplitude fast fluctuations (on the picosecond to nanosecond time scale) that help to overcome the steep energy barrier (*8, 9*).

Although the dynamic properties of several hyperthermophilic−mesophilic enzyme pairs have been compared using a variety of techniques (*3, 10*−*13*), only recently have NMR spectroscopy (*14, 15*) and molecular dynamics simulations (*7, 16, 17*) emerged as the techniques of choice to study protein dynamics, as they allow dynamics to be measured at atomic detail and at different time scales. While several comparative studies have found evidence supporting the hypothesis that hyperthermophilic enzymes are more rigid than their mesophilic counterparts (*3, 7, 18*−*20*), others have not (*14, 16, 21, 22*). The limited amount of experimental data available today, in particular at the residue level, still does not allow us to clearly determine whether rigidity at mesophilic temperatures is a key factor in protein thermostability.

In this study we investigate the relationships between protein conformational flexibility, thermostability, and activity by comparing the backbone amide motions of adenylate kinases (AK)[1] from the mesophile *Escherichia coli* (ECAK) and from the hyperthermophile *Thermotoga neapolitana* (TNAK) using ^{15}N NMR relaxation and NMR-monitored hydrogen−deuterium (H−D) exchange. While ^{15}N relaxation studies provide dynamical information on the fast time scale (picosecond to nanosecond), H−D exchange provides information on slower time scales ($\geq$milliseconds). Although a few mesophilic−hyperthermophilic enzyme pairs have already been compared using these techniques (*8, 9, 18, 23*−*25*), we chose to study TNAK because of its novel and intriguing biochemical characteristics (see below).

AK is a ubiquitous, multidomain enzyme that catalyzes the reversible transfer of ATP's γ-phosphate group to AMP to form ADP. AKs have been thoroughly studied both biochemically and structurally with close to 20 crystal structures of various AKs present in the Protein Data Bank. AKs are formed of three domains: a core, a lid, and an AMP-binding (AMPbd) domain (*26, 27*). A conserved loop, termed the P-loop, essential for nucleotide binding, is also present. In the absence of any ligands, AKs adopt an open form. Based on the structures of ligand-free AKs and on the structures of several AKs complexed with nucleoside monophosphates, nucleoside triphosphates, and inhibitors, it has been inferred that the lid and the AMPbd domain undergo large conformational changes upon binding of the substrates (AMP and ATP) and of the cofactor (Mg^{2+}) (*27*−*30*). The enzyme ternary complex adopts a closed form in which the AMPbd domain closes over AMP and the lid closes over ATP, thereby expelling water to prevent ATP and AMP hydrolyses (*28*).

TNAK shares 44% and 47% identity with ECAK and *Aquifex aeolicus* AK (AAAK), respectively, with most of the ATP and AMP ligands (*26*) (Figure 1) being conserved in TNAK (*31*). The apo and inhibitor-bound crystal structures

[1] Abbreviations: AAAK, *Aquifex aeolicus* adenylate kinase; AK, adenylate kinase; AMPbd domain, AMP-binding domain; Ap5A, P^1, P^5-di(adenosine-5′) pentaphosphate; C4-ECAK, quadruple cysteine mutant ECAK; DSC, differential scanning calorimetry; ECAK, *Escherichia coli* adenylate kinase; H-bond, hydrogen bond; H−D exchange, hydrogen−deuterium exchange; IPTG, isopropyl β-D-thiogalactopyranoside; ITC, isothermal titrating calorimetry; RMSD, root mean square deviation; T_m, melting temperature; TNAK, *Thermotoga neapolitana* adenylate kinase.

of ECAK and AAAK are known (*8, 26, 27*). TNAK also shares high sequence identity with several other bacterial AKs whose structures in complex with various ligands are known [*Bacillus subtilis* AK (BSubAK, 46%), *Bacillus stearothermophilus* AK (BStAK, 45%), and *Bacillus globisporus* AK (BGAK, 43%)]. Biochemical characterization of TNAK showed that it is optimally active at 80 °C and that it is a highly thermostable enzyme with a melting temperature (T_m) of 99.1 °C (*31*), more than 47 °C higher than the 51.8 °C T_m measured for ECAK (*32*). It is the sole enzyme among the 100−200 characterized hyperthermophilic enzymes that shows kinetic properties at 30 °C identical to those of a mesophilic counterpart. Indeed, the kinetic parameters of TNAK at 30 °C are identical to those of ECAK (V_{max}[TNAK] = 1130 μmol min^{-1} mg^{-1}; V_{max}[ECAK] = 1020 μmol min^{-1} mg^{-1}; $K_{m,ATP}$[TNAK] = 49.4 μM; $K_{m,ATP}$[ECAK] = 51 μM; $K_{m,AMP}$[TNAK] = 41 μM; $K_{m,AMP}$[ECAK] = 38 μM) (*31*). Kinetic properties of AAAK, another hyperthermophilic AK, highlight TNAK's unusual behavior: as expected for a hyperthermophilic enzyme AAAK is 9 times less active than ECAK at 20 °C. Only at 50 °C does it become as active as ECAK at 20 °C, and it is maximally active at 80 °C (*24*). AAAK and ECAK dynamics have been compared by ^{15}N NMR relaxation dispersion experiments (*24*) and by ^{15}N NMR relaxation analysis (*8, 9*). Results from these experiments suggest that smaller amplitude, fast fluctuations facilitate large domain movements on the slower time scale (*9*). Together, AAAK and TNAK represent a unique pair of homologous hyperthermophilic enzymes with similar thermal stabilities but different kinetic behaviors at low temperatures. Thus knowing the dynamics of TNAK will be valuable to dissect motions that govern activity and those that govern stability.

In this paper, we use ^{15}N NMR relaxation experiments at 30 °C to determine whether a correlation exists between observed dynamics in the fast time scale (picosecond to nanosecond) and TNAK activity. We compare the dynamics of TNAK in the free and inhibitor-bound forms (the open and closed forms, respectively) to the 30 °C ^{15}N relaxation data for ECAK's free and inhibitor-bound forms (*33*), because dynamics of both conformational states are important for catalysis. We then explore the role slower time scale dynamics plays in the activity and stability of TNAK and ECAK in the millisecond or slower time scale using H−D exchange monitored by NMR through determination of residue-specific protection factors (*P*) in the two proteins. To complete the flexibility mapping of ECAK and TNAK in various time scales, we compare the H−D exchange data for the free and inhibitor-bound forms of both enzymes at 30 °C. Our results are discussed in light of the recent comparison of AAAK and ECAK dynamics (*8, 9*). The two techniques together allow us to address the question: Do the dynamics of TNAK at different time scales explain why this enzyme is highly active at 30 °C? If the hypothesis that enhanced thermostability is attained by enhanced structural rigidity is true, then we expect TNAK to present globally enhanced rigidity with regions of local flexibility that allow activity at low temperatures.

MATERIALS AND METHODS

Protein Expression and Purification. Uniformly labeled recombinant TNAK was overexpressed in *E. coli* BL21(DE3) cells transformed with pTNAK2::Km (*31*). Cells were grown in M9 minimal medium (*34*) containing (i) 1 g/L >98% [^{15}N]ammonium chloride and 2 g/L 99% [$^{13}C_6$]-D-glucose for assignments and (ii) 1 g/L >98% [^{15}N]ammonium chloride and unlabeled glucose for relaxation and H−D exchange measurements. Protein expression was induced at an OD_{600nm} of 1.0−1.2 with 0.4 mM isopropyl β-D-thiogalactopyranoside (IPTG) for 20 h at 37 °C. The previously reported protocol for TNAK purification (*31*) was modified as described below. Supernatant from the heat-treated soluble extract was fractionated with ammonium sulfate at 50% saturation to precipitate impurities. The supernatant was dialyzed against 20 mM Tris-HCl (pH 8.6) (buffer A) and loaded on a Q-Sepharose Fast Flow (Amersham Biosciences, Uppsala, Sweden) anion-exchange column (2.6 × 30 cm, flow rate 2 mL/min) preequilibrated with buffer A. After washing the column with 5 volumes of buffer A, TNAK was eluted with a 400 mL linear 0.2−0.7 M NaCl gradient in buffer A. Fractions containing TNAK were pooled, dialyzed against 20 mM Tris-HCl (pH 8.0) (buffer B), and loaded again on the Q-Sepharose column preequilibrated with buffer B. TNAK was eluted with a 200 mL linear 0−0.7 M NaCl gradient in 50 mM Tris-HCl (pH 7.4). Purified TNAK was concentrated in an ultrafiltration cell equipped with a 10000 molecular weight cutoff membrane (Amicon, Beverly, MA), dialyzed against milliQ water, freeze-dried, and stored at −20 °C.

The *E. coli adk* gene was amplified from *E. coli* K12 genomic DNA and cloned into the pET24a(+) *Nde*I and *Xho*I sites to yield plasmid pECAK1. Uniformly ^{15}N-labeled ECAK was obtained by growing *E. coli* BL21(DE3) (pECAK1) cells in M9 minimal medium containing 1 g/L [^{15}N]ammonium chloride (>98%). ECAK expression was induced by adding 0.4 mM IPTG at an OD_{600nm} of 1.0−1.2. The cells were harvested after 20 h of induction at 37 °C and lysed by two passes through a French pressure cell. The soluble and insoluble fractions were separated by centrifugation at 20000*g* for 20 min. ECAK was purified as described (*35*), except that the protein was eluted from an Affi-Gel Blue gel affinity column (Bio-Rad, Hercules, CA) using a 0−2 M NaCl gradient in 50 mM Tris-HCl (pH 7.4). For the ion-exchange chromatography, a Q-Sepharose Fast Flow column was used instead of DEAE. The purified protein was extensively dialyzed against deionized water with the pH adjusted to the experimental value. It was then lyophilized and stored at −20 °C.

Sample Preparation. (A) NMR Samples. NMR samples of TNAK in the ligand-free form were prepared by dissolving an appropriate amount of freeze-dried TNAK in 320 μL of 50 mM sodium phosphate buffer (pH 7.0) containing 10 μM sodium azide, 6% D_2O/94% H_2O, and protease inhibitor cocktail (Roche, Indianapolis, IN). TNAK concentrations were 1.8 mM for assignment experiments and 1.5 mM for relaxation experiments. For the inhibitor-bound form of the enzyme, TNAK was dissolved in the same buffer, which also contained 8 mM $MgCl_2$ and an appropriate amount of the inhibitor, P^1,P^5-di(adenosine-5′) pentaphosphate (Ap5A).

Final concentrations of TNAK and Ap5A were 1.8 and 5 mM (assignments) and 1.5 and 3 mM (relaxation), respectively.

(B) H−D Exchange Samples. The lyophilized protein samples were dissolved in 50 mM sodium phosphate buffer in D_2O at the desired pH to initiate exchange. In the remainder of the paper, we will use the notation pH* to indicate a pH reading in D_2O without adjustment for the deuterium isotope effect. The final NMR sample contained 2 mM protein (TNAK or ECAK) and 10 μM sodium azide in 320 μL of deuterated buffer. To prepare the inhibitor-bound forms of the proteins (ECAK*Ap5A or TNAK*Ap5A), Ap5A and $MgCl_2$ in D_2O were also added to the mixture at 5 and 8 mM final concentrations, respectively.

NMR Spectroscopy. All NMR experiments, including the H−D exchange experiments, were performed at 30 °C on a Varian Unity Inova 600 spectrometer equipped with triple-resonance probes at 14.1 T.

Sequential Assignments. ^{15}N-HSQC, gradient sensitivity-enhanced triple resonance CBCA(CO)NH, 3D HNCACB, HNCA, and ^{15}N-edited NOESY-HSQC data were collected using established pulse sequences (*36*−*38*). Data were processed using NMRPipe (*39*) and NMRView (*40*). A Gaussian window function in the direct dimension and a shifted sine window function in the two indirect dimensions were applied. Linear prediction was used for the indirect evolution time periods.

Relaxation Measurements. Two-dimensional sensitivity-enhanced NMR experiments were used to measure ^{15}N longitudinal relaxation rates (R_1), transverse relaxation rates (R_2), and heteronuclear ^{15}N−{^{1}H} steady-state NOEs (*41*). The T_1, T_2, and NOE data were acquired with spectral widths of 2200 × 8000 Hz ($F_1 \times F_2$). The number of complex points was 160 × 2048 ($t_1 \times t_2$) for T_1 and NOE and 132 × 2048 for T_2. T_1, T_2, and NOE measurements were performed with 16, 32, and 64 transients per t_1 experiment, respectively. Relaxation delays for R_1 experiments ranged from 0 to 1.8 s and included nine unique time points. The experiments for three time points were repeated twice for error estimation in the measured peak heights. For R_2 measurements, nine unique time points were used, with parametric delays ranging from 0 to 170 ms. Experiments were repeated twice for three of the time points. NOE spectra were recorded with a 3 s predelay for the proton-saturated spectrum and a 6.5 s predelay for the proton-unsaturated spectrum. A 3.5 s saturation period was used for both TNAK and the inhibitor-bound form, TNAK*Ap5A. All spectra were processed using NMRPipe and NMRView.

H−D Exchange Measurements. The following procedure was followed while setting up an exchange experiment to minimize the dead time: (i) a mock sample identical to that used in the exchange experiment was used to tune the NMR probe and adjust the shim settings; (ii) all acquisition parameters were determined using the mock sample; (iii) the exchange experiments were initiated by adding the lyophilized protein in 320 μL of 50 mM sodium phosphate buffer in D_2O preheated to 30 °C, and Ap5A and $MgCl_2$ were added immediately to prepare the inhibitor-bound protein samples; (iv) the solution was then briefly mixed and centrifuged to remove insoluble protein, and the sample was quickly transferred to a shigemi tube; and (v) the lock signal was monitored until it stabilized, shim settings were readjusted with the exchange sample, and data acquisition was initiated. The exchange experiments were performed at two different pH values for each protein conformation. The pH* values measured at the end of the exchange experiments were 7.0 and 7.6 (TNAK), 7.1 and 7.8 (ECAK), 7.0 and 7.5 (TNAK*Ap5A), and 7.0 and 7.6 (ECAK*Ap5A). For each exchange experiment, the start time was taken to be the time of protein−buffer mixing. The dead time of the experiment (i.e., from the time that the protein and buffer were mixed to the start of spectrum recording) was approximately 4−5 min. The last spectrum was recorded 46 h after initiating the exchange. The ^{1}H−^{15}N HSQC spectra were collected with spectral widths of 8000 and 1900 Hz in the ^{1}H and ^{15}N dimensions, respectively. With 32 × 1956 ($t_1 \times t_2$) complex points and four transients per t_1 increment, the total acquisition time for each spectrum was 5 min 18 s.

Relaxation Data Processing and Analysis. Resonance signal intensities were quantified using NMRView. A single exponential function was fitted to the decay curves of T_1 and T_2 peak intensities using CurveFit (A. G. Palmer, Columbia University) to obtain R_1 and R_2 relaxation rates, respectively. Uncertainties in the fitted relaxation rates were estimated using a jackknife algorithm. Experimental peak uncertainties were determined from the duplicate time points. Steady-state NOEs were calculated as the ratio of cross-peak heights of the saturated and unsaturated protons. The average percentage errors for TNAK's R_1, R_2, and NOE values were 2.7%, 1.6%, and 5%, respectively. The average percentage errors for TNAK*Ap5A's R_1, R_2, and NOE values were 2.6%, 1.1%, and 4.6%, respectively.

Relaxation rates and NOEs were fitted to the Lipari−Szabo model-free formalism (*23, 42*−*45*) using the ModelFree 4.0 software (*46*). Although Meirovitch and co-workers have advocated the use of mode-coupled slowly relaxing local structure (SRLS) analysis for AK (*47*), Henzler-Wildman and co-workers (*9*) have shown that, for AK, complex correlated domain motions do not significantly affect the order parameters obtained from model-free analysis, provided microsecond to millisecond time scale exchange contributions to R_2 values have been removed. Inertial tensor analyses of TNAK and TNAK*Ap5A were performed using TNAK and TNAK*Ap5A homology models (see Structure Coordinates) as input PDB files. Hydrogen atoms were added using InsightII (Accelrys, San Diego, CA). The inertia tensor calculations were performed using PDBINERTIA from the ModelFree 4.0 package (*23, 46*), and the hydrodynamic calculations were performed using the HYDRO suite of programs (*48*).

The R_2/R_1 ratios of a subset of rigid NH vectors (which have negligible components of internal motions and/or exchange contributions to the ^{15}N relaxation rates) were selected for calculating the principal components and the orientation of the diffusion tensors of TNAK and TNAK*Ap5A. Residues were selected if their NOE values were >0.7 and

$$(\langle T_2\rangle - T_{2,n})/\langle T_2\rangle - (\langle T_1\rangle - T_{1,n})/\langle T_1\rangle < 1.5\mathrm{SD} \quad (1)$$

where $\langle T_2\rangle$ is average T_2 and where $T_{2,n}$ is the T_2 value of residue n. SD is the standard deviation of the function $(\langle T_2\rangle - T_{2,n})/\langle T_2\rangle - (\langle T_1\rangle - T_{1,n})/\langle T_1\rangle$ (*49*). Components of the overall rotational diffusion tensor were determined using local diffusion approximation as implemented in the Quadric Diffusion software by Palmer et al. (*23, 46*). To choose the

best-fit model to describe the molecular rotational diffusion, *F*-statistic testing was used to compare isotropic, axially symmetric, and anisotropic diffusion models.

Following model selection, individual NH data were fitted to each of the five motional models described by Mandel et al. (*23*). The difference between parallel and perpendicular components of the ^{15}N chemical shift tensor ($\Delta\sigma$) was taken to be −160 ppm, and the N−H internuclear distance was assumed to be 1.02 Å (*50*). Fitting procedures, model selection criteria, and optimization procedures were performed as described (*23*). A model was selected by comparing the value of the χ^2 function at a critical value, α, of 0.1 with the simulated critical value. *F*-statistical testing (with $\alpha = 0.2$) was used to determine if the more complicated model fit the data better for each spin. Monte Carlo simulations were performed using 500 randomly distributed synthetic data to determine uncertainties in the fitted model-free parameters. The internal model-free parameters for each residue were further optimized simultaneously with the global correlation time. The procedure was iterated until the results converged.

H−D Exchange Rate Analysis. A Gaussian window function in the direct dimension and a sine window function in the indirect dimension were applied. Phase and baseline corrections were used in all cases. The HSQC spectra were zero-filled to 2048 × 512 data points in ^1H and ^{15}N dimensions, respectively. The H−D exchange rates were quantified using the intensity of the $^1H-^{15}N$ amide cross-peaks in a series of HSQC spectra recorded at different times. For each amide, i, the time dependency of peak intensity was fitted to a single exponential decay function equation, $I(t) = I_0(t) + I_i \exp(-k_{ext})$, using CurveFit. For each amide proton at 30 °C and at a specific pH, the intrinsic rate constant (the Bai factor), k_{ch}, was predicted from the protein sequence using the program HXPrep (courtesy of Zhonggyi Zhang), which uses the procedure described by Bai et al. (*51*). The calculated k_{ch} values and the measured k_{ex} values were used to calculate the protection factors. The theory underlying EX1 and EX2 exchange mechanisms is described elsewhere (*52*−*54*).

Structure Coordinates. A three-dimensional structure of TNAK is not available at this time. A comparison of bacterial AK structures shows that the AK fold is highly conserved. With sequence identity above 40%, homology modeling can produce structures that are equivalent to a medium resolution crystal structure in many respects. Since calculations for axially symmetric diffusion tensors take into account the orientations of the N−H bond vectors relative to the principal axes of the diffusion tensor, the input structure is important. Superposition of several closed forms of AK [BGAK*Ap5A (PDB code 1s3g), BSubAK*Ap5A (PDB code 1p3j), BStAK*Ap5A (PDB code 1zin), and ECAK*Ap5A (PDB code 1ake)] shows the structures to be highly similar [root mean square deviation (RMSD) within 1.6 Å], with obvious differences only in the position of the lid and in the C-terminus. The two available AK open forms [AAAK (PDB code 2rh5) and ECAK (PDB code 4ake)] also show striking structural similarities in their cores with differences localized to the lid and to the base of the AMPbd domain. In fact, the crystal structure of apo-AAAK reveals three different lid conformations for the three molecules in the asymmetric unit, indicating that the lid samples conformations along the trajectory from open to closed substates in solution (*8, 9*). Order parameters calculated from the three apo-AAAK structures as well as from molecular dynamic simulation sampling a wide range of lid conformations resulted in S^2 values that agreed with experimental values (*9*). The RMSDs between our open TNAK 3D model and ECAK and between our closed TNAK*Ap5A 3D model and ECAK*Ap5A were 0.9 and 1.7 Å, respectively. These RMSD values are in the range of those observed between experimentally determined AK structures. On the basis of these considerations, we argue that the TNAK structure derived from homology modeling is of high quality and is good for the purpose of our investigations.

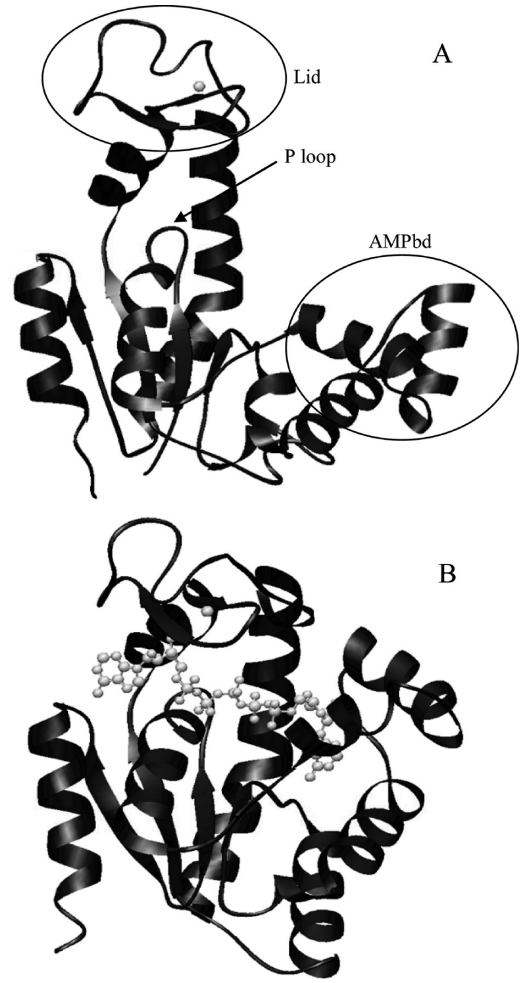

FIGURE 2: Ribbon diagrams of the homology-modeled structures of (A) TNAK (open form) and (B) TNAK*Ap5A (closed form). The lid, the AMPbd domain, and the P-loop are indicated in the open form. Zn^{2+} in the lid domain and Ap5A are shown with a ball and stick representation. The figures were generated using the program Ribbons.

Three-dimensional models of TNAK in both the open and closed forms were built by comparative modeling using Modeler software (Figure 2) (*55*). TNAK*Ap5A was modeled using the structures of BSubAK*Ap5A, BGAK*Ap5A, and BStAK*Ap5A as templates. BGAK, BSubAK, and BStAK share 43%, 46%, and 45% identity with TNAK, respectively, and all four AKs contain a structural Zn^{2+} in their lid (*31*). TNAK was modeled using the structures of ECAK (PDB code 4ake) and BStAK*Ap5A as templates.

AKs consist of three domains and two pairs of bending regions, one between the AMPbd domain and core (i.e.,

AMPbd−core hinges) and the other between lid and core (i.e., lid−core hinges). In ECAK the AMPbd domain contains residues 31−72, the lid contains residues 119−156, and the core is formed by residues 1−28, 80−112, and 173−214. The AMPbd−core hinges involve residues 29, 30, and 73−79, and the lid−core hinges consist of residues 113−118 and 157−172 (*56*). The corresponding residues in TNAK domains are as follows: (i) core, 1−30, 83−119, and 180−220; (ii) AMPbd domain, 33−75; (iii) lid, 126−163; (iv) AMPbd−core hinges, 31, 32, and 76−82; and (v) lid−core hinges, 120−125 and 163−179.

Differential Scanning Calorimetry. Differential scanning calorimetry (DSC) was performed with ECAK (at 0.19 mg/mL) and TNAK (at 0.1 mg/mL) in the presence or absence of Ap5A using a VP-DSC calorimeter (Microcal, Northampton, MA). These protein concentrations were chosen to minimize skewing of T_m peaks by protein aggregation observed above T_m at higher protein concentrations. All protein solutions and reference buffer samples analyzed contained 50 mM sodium phosphate buffer (pH 7.0) plus 2 mM Mg^{2+} for enzyme runs in the presence of Ap5A. Sample solutions were degassed and thermally equilibrated for 30 min under vacuum while stirring prior to loading. Replicate DSC scans of each protein solution were performed from 20 to 130 °C at a 45 °C/h scan rate. DSC results were analyzed using the Origin 7.0 software package (Microcal).

TNAK's binding affinity for Ap5A was measured at 30 °C by isothermal titrating calorimetry (ITC) on a VP-ITC calorimeter (Microcal). Solutions of TNAK (20 μM), Ap5A (400 μM), and buffer blank were in 50 mM sodium phosphate buffer, pH 7.0, containing 2 mM Mg^{2+}. ITC experiments consisted of a series of 29 injections of Ap5A solution (10 μL injections at 0.5 μL/s) into the TNAK solution within the sample cell at 6 min intervals with 300 rpm stirring. Data analysis of the binding isotherm was performed using Origin 7.0 using the "one set of sites" binding model.

RESULTS

*Melting Temperatures of ECAK, ECAK*Ap5A, TNAK, and TNAK*Ap5A.* The T_ms of TNAK (99 °C) and ECAK (52 °C) obtained by DSC in this study (data not shown) were very similar to the previously published values of 99.1 °C for TNAK (*31*) and 51.8 °C for ECAK (*32*). ECAK complexed with the tight inhibitor Ap5A had a T_m of 62.5 °C, while the T_m of TNAK*Ap5A was 99 °C.

ITC experiments performed at 30 °C in the same buffer conditions as the DSC experiments confirmed that Ap5A binds to TNAK (as evidenced by the curvature of the ITC isotherm, not shown) with an 8 μM dissociation constant. Ap5A's equilibrium binding was achieved within a few minutes. These results indicate that TNAK*Ap5A's T_m of 99 °C (identical to TNAK's T_m) is not due to Ap5A's inability to bind the enzyme.

Resonance Assignments of TNAK. TNAK contains 220 residues, 10 of which are prolines that are not detectable in a 2D $^1H-^{15}N$ HSQC (Supporting Information Figure S1). ^1H and ^{15}N backbone resonances of 197 out of the 210 nonproline residues were assigned in ligand-free TNAK. The two N-terminal residues (M1 and M2) and the C-terminal residue (K220), as well as five P-loop residues and three lid residues, are among the 13 residues whose correlations could not be detected in the HSQC spectrum. Among the 197 residues with detectable resonances, eight pairs of residues (L5 and Q162, Y178 and H30, I67 and V55, I22 and K50, A19 and V177, D155 and D187, L66 and V185, and K58 and D166) generated peaks that overlapped with each other. With TNAK*Ap5A, 193 peaks were seen in the HSQC spectrum (Supporting Information Figure S2) out of the expected 210. Five of the 17 missing residues are located in the P-loop; 2 are the N-terminal residues, M1 and M2; and 2 are the C-terminal residues D219 and K220. Three correlations from residues in the lid and four from residues in the AMPbd domain are also missing. Of the 193 correlations that are detected in the TNAK*Ap5A HSQC spectrum, nine pairs of residues (L75 and R91, L61 and R126, R38 and E57, K72 and L179, V123 and S218, K78 and L99, K53 and D117, A94 and I204, and L48 and W217) and three triplets of residues (K43, D187, and K213; K42, V67, and Q95; and H30, R74, and K176) generated overlapping peaks. TNAK and TNAK*Ap5A HSQC spectra differed considerably from each other (Supporting Information Figures S1 and S2), emphasizing the fact that large conformational changes are induced by inhibitor binding, as has already been observed for ECAK (*33*).

Secondary structural elements could be readily detected in the 3D ^{15}N-edited NOESY-HSQC spectrum through NOE connectivities. The α-helices and β-strands identified in TNAK and TNAK*Ap5A by NMR correlated well with those predicted by the 3D models.

Relaxation Data. Excluding residues with overlapping or weak correlation peaks, 177 residues were used for TNAK's relaxation data analysis. For TNAK*Ap5A, 164 residues were used for the analysis after excluding 27 residues with overlapping cross-peaks and 2 residues with weak cross-peaks. The R_1, R_2, and $^{15}N-\{^1H\}$ NOE values of TNAK and TNAK*Ap5A residues are shown in panels a, b, and c of Figure 3, respectively. The 10% trimmed mean values of R_1, R_2, and $^{15}N-\{^1H\}$ NOE values of TNAK (TNAK*Ap5A) are 0.93 ± 0.023 s^{-1} (1.01 ± 0.024 s^{-1}), 20.53 ± 0.30 s^{-1} (18.32 ± 0.17 s^{-1}), and 0.87 ± 0.039 (0.81 ± 0.017), respectively. Low NOE values reflect the presence of considerable motions on the fast time scale (picosecond to nanosecond). As expected from the movements of the lid and AMPbd domain triggered by substrates or inhibitor binding in AKs, and as expected from the low NOE values in the ECAK free enzyme, TNAK's lid and AMPbd domain show NOE values that are lower than those of the rest of the protein. TNAK*Ap5A's lid and AMPbd domain also show low NOE values, suggesting that high-frequency motions are not suppressed in the lid and AMPbd domain upon inhibitor binding. This trend in NOE values is unlike that seen for ECAK, where the NOE values become uniformly high throughout the backbone upon inhibitor binding (*33*), indicating that high-frequency motions in ECAK's lid and AMPbd domain are largely suppressed upon inhibitor binding.

Molecular Rotational Diffusion from Hydrodynamic Calculations and NMR Data. The ratios of TNAK's principal moments were 1.0:0.88:0.529. Modeling TNAK as a prolate ellipsoid yielded the Perrin shape factors $F_a = 0.834$ and $F_c = 1.335$. The R_2/R_1 ratios for 112 residues not subject to large amplitude fast internal motions or to slow time scale

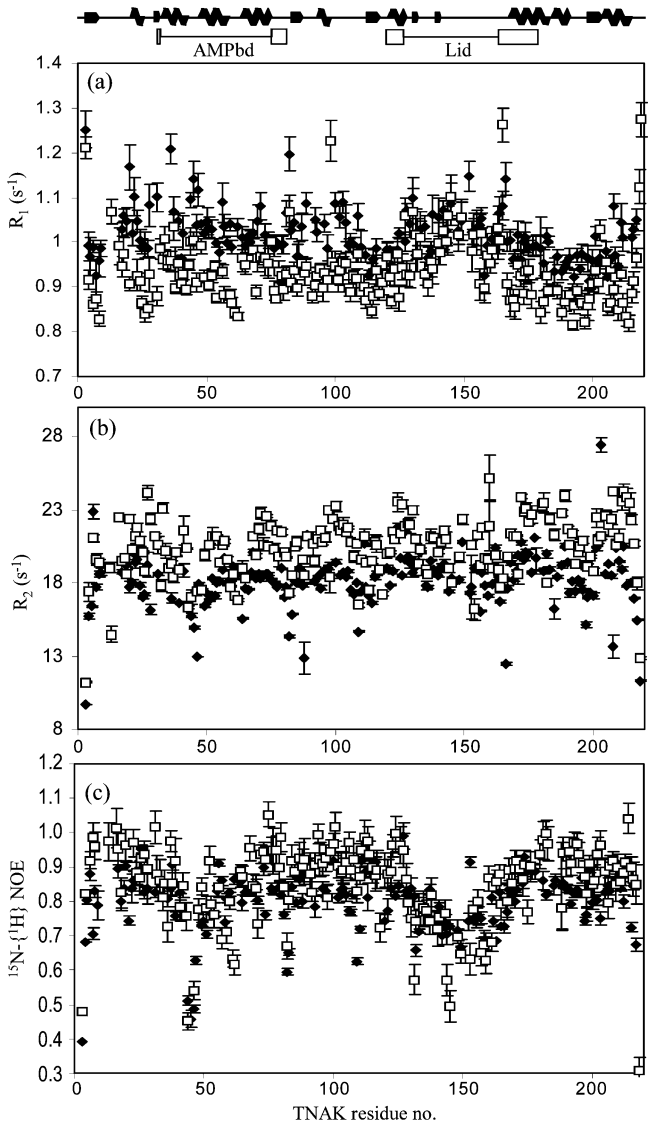

FIGURE 3: Relaxation parameters of TNAK (□) and TNAK*Ap5A (◆): (a) R_1, (b) R_2, and (c) $^{15}N-\{^1H\}$ NOE. The locations of TNAK secondary structures and domains are indicated on top of the figure. The open rectangles show the hinge regions framing the AMPbd and lid domains.

conformational exchange were used to estimate the components of the rotational diffusion tensor. The axially symmetric model agreed significantly better ($p < 0.025$) with the experimental data than the isotropic model did, according to an *F*-statistic test ($F = 18.4$). Because the fitting improvement for the fully anisotropic model relative to the axially symmetric model was not significant ($F = 0.021$), the prolate model was selected as the best fit to the data. After selecting the appropriate models for the individual NH vectors and optimizing the parameters in model-free calculations, the final τ_c was 14.88 ± 0.021 ns with a $D_{||}/D_{\perp}$ ratio of 1.2 ± 0.01. These values agreed well with the τ_c (15.26 ns) and $D_{||}/D_{\perp}$ (1.26) values predicted from the structure and molecular weight of TNAK using hydrodynamic calculations.

The inertia tensor for TNAK*Ap5A using the homology-modeled structure has principal moments with the ratio 1:0.88:0.75. A rotational correlation time, τ_c, of 13.16 ns and a $D_{||}/D_{\perp}$ ratio of 1.1 were calculated for TNAK*Ap5A with a molecular mass of 24.8 kDa using hydrodynamic calculations. The R_2/R_1 data of 110 spins selected using the criteria described in Materials and Methods were used to estimate the diffusion tensor parameters. The axially symmetric and the fully anisotropic tensors fitted the data better than the isotropic tensor did, but the two models could not be distinguished statistically using an *F*-test. Therefore, the simpler, axially symmetric oblate model was chosen. After optimizing the model-free parameters, the final τ_c and $D_{||}/D_{\perp}$ values were 13.56 ± 0.03 and 0.87 ± 0.009, respectively.

The possibility of protein self-association at such high concentrations (1.8 mM) must be considered, because protein self-association can adversely affect τ_c values and relaxation parameters. We do not believe that aggregation occurred in the TNAK and TNAK*Ap5A NMR samples because (i) the TNAK and TNAK*Ap5A τ_c values (14.88 and 13.6 ns, respectively) are close to the estimated τ_c, based on hydrodynamic calculations (15.26 ns for TNAK and 13.16 ns for TNAK*Ap5A), and they agree quite well with the molecular size and anisotropy of the protein; and (ii) similar τ_c values were calculated for ECAK and ECAK*Ap5A (15.05 and 11.4 ns, respectively) from R_2/R_1 data (*33*). Since ECAK and TNAK are close in size and shape, similar τ_c values suggest that monomers are predominant in both the TNAK and TNAK*Ap5A samples.

Backbone Internal Motions. The relaxation parameters of 112, 9, 32, 3, and 21 TNAK residues were fitted to motional models 1, 2, 3, 4, and 5, respectively. Contrast this with ECAK, where the relaxation parameters of 2, 109, 7, 48, and 21 residues were fitted to models 1, 2, 3, 4, and 5, respectively. The fact that the majority of ECAK residues were fitted to model 2 (with parameters S^2 and τ_e) rather than model 1 (only S^2) indicates a higher rigidity for many residues in TNAK. This effect is less pronounced for the inhibitor-bound enzymes: the relaxation parameters of 84, 27, 35, 3, and 15 TNAK*Ap5A residues were fitted to models 1, 2, 3, 4, and 5, respectively, while those of 66, 59, 39, 5, and 30 in ECAK*Ap5A residues were fitted to models 1, 2, 3, 4, and 5, respectively.

Picosecond to Nanosecond Time Scale Motions. ECAK and TNAK's generalized order parameter (S^2) values are plotted as a function of residue number in Figure 4a. A consistent increase in S^2 values is observed for most TNAK residues compared to the corresponding ECAK residues, indicating that the amplitude of internal motions in the picosecond to nanosecond time scale is larger in ECAK than in TNAK. Comparison of AAAK and ECAK at 20 °C yielded a similar result: significantly lower S^2 values for ECAK residues relative to AAAK residues (*9*). Although S^2 values are uniformly higher in TNAK than in ECAK, a number of TNAK residues differ from this general behavior. Many of these residues are clustered in TNAK's lid, AMPbd domain, and hinge regions. Residues 43−62 in the AMPbd domain have low S^2 values in both ECAK and TNAK. The S^2 values of residues 161, 162, 165−169, and 171 in TNAK's lid are also as low as those of the corresponding ECAK residues. Our results are consistent with the observations of Henzler-Wildman et al. for ECAK and AAAK in their open forms (*9*). Many residues with low S^2 values are located in ECAK regions that are involved in conformational changes. While AAAK has higher order parameters than ECAK in these regions at 20 °C, S^2 values are closer at temperatures where ECAK and AAAK have comparable activities.

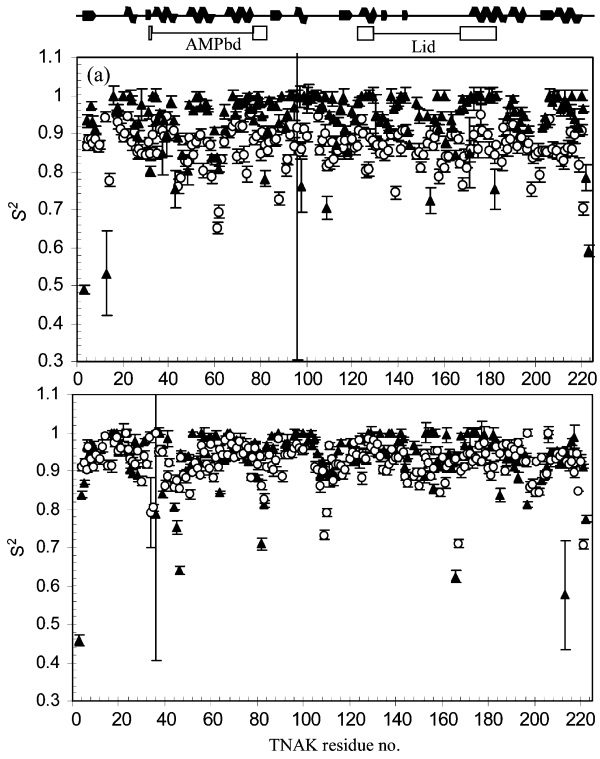

FIGURE 4: Order parameters, S^2, at 30 °C: (a) TNAK (▲) and ECAK (○) and (b) TNAK*Ap5A (▲) and ECAK*Ap5A (○). ECAK data (*33, 47, 58*) are plotted as per the sequence alignment shown in Figure 1. TNAK secondary structures and domains are indicated on top of the figure. The open boxes show the hinge regions framing the AMPbd and lid domains.

In contrast to the enzyme open forms, ECAK*Ap5A and TNAK*Ap5A show only little differences in S^2 values (Figure 4b). The trend in S^2 values along the backbone closely matches for the two enzymes, with low S^2 values for a number of hinge residues in ECAK*Ap5A and TNAK*Ap5A (e.g., 80−83, 109, and 166 in TNAK*Ap5A). TNAK*Ap5A also contains regions that show greater flexibility than the rest of the backbone. In particular, residues in the AMPbd domain have lower S^2 values than the corresponding residues in ECAK*Ap5A.

We calculated mean S^2 values ($\langle S^2 \rangle$) for each domain and hinge regions in ECAK, ECAK*Ap5A, TNAK, and TNAK*Ap5A to determine the relative rigidity of each of these domains. We also calculated $\langle S^2 \rangle$ values for each secondary structural element in the four enzymes (Table 1). From Table 1, the following can be noted: (i) The overall $\langle S^2 \rangle$ values of the core, lid, and AMPbd domain are similar to one another in each of the four enzyme forms, indicating similar overall rigidity on the picosecond to nanosecond time scale across the whole protein. (ii) The percentage increases in the overall $\langle S^2 \rangle$ values of the three TNAK domains (compared to ECAK) are similar (between 7.7% and 9.5%), indicating uniformly higher rigidity in TNAK. In other words, each domain contributes to a similar extent to TNAK's overall higher rigidity. (iii) In contrast, the overall $\langle S^2 \rangle$ values of the three TNAK*Ap5A domains are similar to those of ECAK*Ap5A, indicating similar levels of rigidity on the picosecond to nanosecond time scale for both inhibitor-bound enzymes.

While all TNAK secondary structural elements show higher $\langle S^2 \rangle$ values than the corresponding ECAK elements, the most significant $\langle S^2 \rangle$ increases are in TNAK's core (in particular in β9, α5, and α9). Additionally, α3 and α4 in the AMPbd domain, β6 in the lid, and α6 in one of the two lid−core hinges also show higher $\langle S^2 \rangle$ values. In contrast, most secondary structural elements in ECAK*Ap5A and TNAK*Ap5A show similar $\langle S^2 \rangle$ values. Loops in the AMPbd domain have among the lowest $\langle S^2 \rangle$ values of any secondary structural elements in TNAK, TNAK*Ap5A, and ECAK. Interestingly, the significant 12% $\langle S^2 \rangle$ increase seen in ECAK AMPbd loops upon inhibitor binding is not seen between TNAK and TNAK*Ap5A. TNAK*Ap5A AMPbd loops $\langle S^2 \rangle$ remain similar to that of TNAK, indicating similar dynamic characteristics of these loops in TNAK's open and closed forms. In ECAK*Ap5A and TNAK*Ap5A, the loops belonging to the lid−core hinges have among the lowest $\langle S^2 \rangle$ values, suggesting that the hinges become especially flexible in the closed state.

As in ECAK, TNAK's AMPbd domain has the highest density of residues whose motions are best described by model 5, featuring motions on multiple time scales (nanosecond and subnanosecond). In TNAK, another cluster of residues that show model 5 type motions is located in the lid and the lid−core hinge following the lid. Complex motional modes were also observed for AAAK's lid, AMPbd domain, and hinges at 50 and 80 °C, substantiating the evidence for flexibility of these regions (*9*).

Microsecond Time Scale Motions. Microsecond to millisecond time scale motions are identified by the parameter R_{ex}, which represents exchange contribution to T_2. R_{ex} indicates exchange between conformational states that sense different chemical environments. Because TNAK and TNAK*Ap5A's three-dimensional structures have not been determined experimentally, and because R_{ex} values based on model-free analysis have to be interpreted cautiously, only overall differences between the proteins are presented. Localized differences involving specific residues are not discussed.

Residues showing exchange contributions are illustrated in Figure 5a (TNAK and ECAK) and Figure 5b (TNAK*Ap5A and ECAK*Ap5A). Not shown are the dynamics of several TNAK and TNAK*Ap5A P-loop residues, which could not be analyzed due to large line widths attributable to exchange broadening. Twice as many residues in ECAK (45) than in TNAK (22) show exchange contributions at 30 °C. In contrast, almost as few ECAK*Ap5A residues (17) show microsecond time scale motion as in TNAK*Ap5A (14). ECAK, TNAK, ECAK*Ap5A, and TNAK*Ap5A residues with $R_{ex} > 1.5\ s^{-1}$ are listed in Table 2. The predominant differences in microsecond time scale motions between TNAK and ECAK lie in the core and in the loops of the lid−core hinges. Specifically, the core β-strands have no exchange contribution in TNAK, while three of the four ECAK core β-strands have residues with R_{ex} values above $1.5\ s^{-1}$, again reinforcing the high rigidity of TNAK's core. Upon inhibitor binding, ECAK's core is significantly rigidified in the microsecond time scale, as was also observed in the picosecond to nanosecond time scale. Twenty of the 22 residues in ECAK's core β-strands and α-helices that had R_{ex} values in ECAK do not have R_{ex} values in ECAK*Ap5A. In contrast, TNAK*Ap5A's core shows similar rigidity as TNAK's.

Several residues in ECAK and TNAK's AMPbd and lid domains show microsecond time scale chemical exchange.

Table 1: Average S^2 Values, $\langle S^2 \rangle$, of the Secondary Structures in the Various Domains of ECAK, TNAK, ECAK*Ap5A, and TNAK*Ap5A

		ECAK[a]		TNAK		ECAK*Ap5A[a]		TNAK*Ap5A	
domain	secondary structure	$\langle S^2 \rangle^b$	N^c	$\langle S^2 \rangle^b$	N^c	$\langle S^2 \rangle^b$	N^c	$\langle S^2 \rangle^b$	N^c
core	β1	0.88 (0.01)	6	0.94 (0.03)	4	0.92 (0.02)	6	0.91 (0.06)	6
	β2	0.89 (0.01)	4	0.96 (0.03)	4	0.92 (0.02)	4	0.94 (0.07)	5
	β3	0.86 (0.02)	6	0.93 (0.04)	6	0.91 (0.02)	6	0.93 (0.04)	5
	β8	0.84 (0.02)	6	0.96 (0.03)	6	0.88 (0.04)	6	0.93 (0.04)	6
	α1	0.90 (0.04)	5	0.95 (0.05)	4	0.95 (0.03)	5	0.95 (0.04)	6
	α5	0.89 (0.03)	8	0.99 (0.01)	5	0.95 (0.02)	8	0.99 (0.01)	3
	α8	0.89 (0.04)	10	0.97 (0.02)	4	0.95 (0.02)	11	0.92 (0.04)	9
	α9	0.86 (0.06)	12	0.97 (0.03)	11	0.91 (0.07)	13	0.91 (0.04)	9
	loops	0.87 (0.06)	30	0.93 (0.07)	35	0.92 (0.06)	31	0.93 (0.07)	31
	average	0.873		0.947		0.92		0.93	
AMPbd	α2	0.90 (0.03)	10	0.92 (0.08)	10	0.91 (0.08)	10	0.93 (0.10)	5
	α3	0.86 (0.03)	10	0.95 (0.06)	8	0.90 (0.04)	10	0.95 (0.04)	9
	α4	0.89 (0.04)	11	0.98 (0.03)	10	0.96 (0.02)	11	0.95 (0.05)	10
	loops	0.80 (0.09)	9	0.85 (0.04)	6	0.91 (0.04)	10	0.87 (0.16)	5
	average	0.865		0.932		0.92		0.933	
lid	β5	0.86 (0.01)	4	0.94 (0.01)	3	0.96 (0.06)	4	0.97 (0.02)	3
	β6	0.83 (0.08)	3	0.98	2	0.94 (0.01)	4	0.97	2
	β7	0.88	1	−[e]		0.94	2	−[e]	
	β8	0.80	2	−[e]		0.90	2	−[e]	
	loops	0.86 (0.04)	20	0.93 (0.07)	19	0.91 (0.03)	22	0.96 (0.04)	23
	average	0.854		0.935		0.921		0.962	
AMPbd−core hinges[d]	loops	0.88 (0.03)	8	0.92 (0.08)	9	0.92 (0.03)	9	0.91 (0.09)	7
lid−core hinges[d]	α6	0.87 (0.05)	9	0.98 (0.02)	8	0.95 (0.03)	9	0.96 (0.03)	7
	α7	0.86 (0.05)	12	0.96 (0.08)	12	0.93 (0.02)	15	0.98 (0.02)	12
	loops	0.87 (0.05)	3	0.91 (0.05)	3	0.86 (0.13)	3	0.85 (0.15)	4
	average	0.865		0.96		0.93		0.95	

[a] ECAK and ECAK*Ap5A data are from Shapiro et al. (*33*). [b] Standard deviation is in parentheses. [c] Number of residues included in the average. [d] Regions defined by Hayward (*56*). [e] β7 and β8 are not predicted in the TNAK and TNAK*Ap5A models.

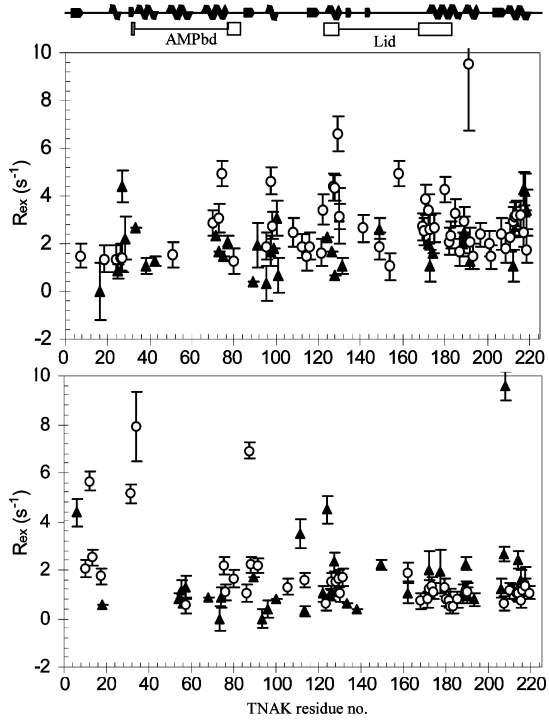

FIGURE 5: Exchange contributions, R_{ex} (s^{-1}), of (a) TNAK (▲) and ECAK (○) and (b) TNAK*Ap5A (▲) and ECAK*Ap5A (○) at 30 °C. ECAK data (*33, 47, 58*) are plotted as per the sequence alignment shown in Figure 1. TNAK secondary structures and domains are indicated on top of the figure. The open rectangles show the hinge regions framing the AMPbd and lid domains.

In both enzymes, the AMPbd domain becomes more rigid upon inhibitor binding, with a single AMPbd domain residue showing any chemical exchange in ECAK*Ap5A and none in TNAK*Ap5A. In contrast, several residues in ECAK*Ap5A's AMPbd−core hinges show significant mobility. The lid domains of ECAK and TNAK inhibitor-bound forms also have several residues (some of them the same as in the free forms) that show significant R_{ex} values. A notable difference between ECAK*Ap5A and TNAK*Ap5A lies in the lid−core hinges. Whereas the lid−core hinges have 10 residues with R_{ex} values in ECAK, they have none in ECAK*Ap5A. In contrast, the same residues in TNAK and TNAK*Ap5A's lid−core hinges show R_{ex} values, indicating that these regions are flexible in both TNAK forms.

The H−D Exchange Mechanism at the Experimental pH Values.* Local and global unfolding−refolding motions involving hydrogen bond (H-bond) breakage occur on time scales slower than seconds. These motions were investigated in ECAK, ECAK*Ap5A, TNAK, and TNAK*Ap5A by native state H−D exchange followed by collecting $^1H-^{15}N$ HSQC NMR spectra at different time points for 46 h. Exchange experiments were performed at two pH values for each protein. TNAK is most stable between pH 7.0 and pH 8.5, and its activity at pH 6.5 drops to 50% of its optimal activity at pH 7.5 (*31*). For these reasons, we chose 7.0 and 8.0 as the target experimental pH values for the two enzymes. The final pH* of the deuterated samples were 7.0 and 7.6 for TNAK and 7.1 and 7.8 for ECAK. Twenty-four of the ECAK amide protons with measurable exchange rates showed EX2 exchange, with higher exchange rates at pH* 7.8 than at pH* 7.1. The ratio of exchange rates for these amide protons at pH* 7.8 and pH* 7.1 was consistent with a 10-fold increase in exchange rate for every pH unit increase

Table 2: Residues with R_{ex} Values >1.5 s^{-1} in the Various Domains of ECAK, TNAK, ECAK*Ap5A, and TNAK*Ap5A

domain	secondary structure	ECAK residues[a]	TNAK residues	ECAK*Ap5A residues[a]	TNAK*Ap5A residues
core	β1	5	−	−	6
	β3	−	−	84	−
	β4	105, 109	−	106	−
	β9	194	−	−	−
	α5	92, 94, 95	97	−	−
	α8	178, 180, 182, 184, 185	188, 189	−	189
	α9	202, 204, 205, 206, 207, 209, 210, 212	208, 212, 213, 214	−	209, 210, 212
	loop	101, 176, 190, 200	27, 28, 91, 99, 100	8, 10, 11, 15, 85, 88	89, 111, 202, 203
AMPbd	α2	−	33	32	−
	α3	48	−	−	−
	α4	67, 70, 71	71, 73	−	−
lid	α6	120, 121	126	119, 121	127
	β5	123	130	124	−
	β6	134	−	−	−
	β8	151	−	−[c]	−[c]
	loop	122, 142	149	122, 155	149
AMPbd−core hinges[b]	loop	−	77	29, 72, 77	−
lid−core hinges[b]	α6	114, 115	124	−	124
	α7	162, 163, 164, 165, 166, 168, 173, 175	172, 174	−	172, 177

[a] ECAK and ECAK*Ap5A data are from Shapiro et al. (*33*). [b] Regions defined by Hayward (*56*). [c] β8 is not predicted in the TNAK and TNAK*Ap5A models.

(i.e., the pH-dependent increase expected for EX2 exchange mechanism) (*52, 53*). Fourteen ECAK amide protons showed similar exchange rates at the two pH* values, indicating that these protons likely exchange via the EX1 mechanism. Similarly, 20 TNAK amide protons did not show any difference in their exchange rates, within error, at pH* 7.0 and pH* 7.6, indicating an EX1 exchange mechanism for these protons. All other 23 TNAK amide protons with measurable exchange rates showed EX2 exchange in these conditions. The pH dependence of exchange rates was also determined for ECAK*Ap5A and TNAK*Ap5A. The pH* values of the deuterated samples were 7.0 and 7.5 for TNAK*Ap5A and 7.0 and 7.6 for ECAK*Ap5A. As for the ligand-free proteins, 19 of 47 ECAK*Ap5A amide protons and 28 of 41 TNAK*Ap5A amide protons did not show any pH-dependent exchange rate variation. The exchange rates reported at the two pHs indicate that some residues are likely to exchange with the EX1 mechanism or have an exchange mechanism between EX1 and EX2.

Determination of P Values. The residue-specific exchange rates (k_{obs}) determined by fitting a single exponential function to peak intensities were used to determine residue-specific protection factors P (*52*−*54*). P values were obtained from the relation $P = k_{ch}/k_{obs,}$ where k_{ch} is the amides' intrinsic exchange rate (*51*). The P values reported and discussed in this work were calculated from the exchange data collected at pH* 7.0. Protection factors were calculated for only those amide protons with measurable exchange rates (a number of amide protons exchanged within the dead time of the experiment, whereas others remained unexchanged during the time course of the experiments). Exchange data for 75, 70, 60, and 93 residues in ECAK, TNAK, ECAK*Ap5A, and TNAK*Ap5A, respectively, could not be obtained. Two reasons account for the missing exchange data: One, not all residues could be detected in the HSQC spectrum during the initial NMR assignments of ECAK [202 assigned (*57, 58*)], ECAK*Ap5A [191 assigned (*57*))], TNAK (197 assigned), and TNAK*Ap5A (193 assigned). Two, since HSQC spectra for the exchange experiments were recorded for only 5 min, resolution was compromised and several cross-peaks overlapped. H−D exchange rates for overlapping peaks were not quantified.

The percentages reported in this paragraph were calculated based on the total number of residues having exchange data, rather than on the number of residues in the protein. Overall, TNAK has a significantly higher percentage of unexchanged residues (20%) than ECAK (12%). Conversely, a smaller percentage of TNAK residues (51%) exchange in the dead time of the experiment than ECAK residues (64%). If unexchanged residues are indicative of high conformational rigidity, and if very fast exchange indicates high flexibility, these results show that TNAK is more rigid than ECAK. Although the increase in percentage of protected amides in ECAK*Ap5A relative to ECAK is modest (only 3%), the percentage of unexchanged amide protons increases significantly (by 7%) from ECAK to ECAK*Ap5A, implying increased rigidity for the inhibitor-bound enzyme. The increases in the percentages of unexchanged amides (2%) and amides with some protection factor (3%) from TNAK to TNAK*Ap5A are smaller than between ECAK and ECAK*Ap5A. Still, they suggest that TNAK*Ap5A is at least as rigid, if not more rigid, than TNAK. Not surprisingly, TNAK*Ap5A is more rigid overall than ECAK*Ap5A (54% of the amides are protected in TNAK*Ap5A vs 46% in ECAK*Ap5A).

Slow Hydrogen Bond-Breaking Motions. The log P values for ECAK and TNAK residues with measurable amide proton exchange rates are shown in panels a and b of Figure 6. Residues whose amide protons exchanged within the dead time of the NMR experiments were arbitrarily given a log P value of 0.1, indicating rapid exchange, to distinguish them from amide protons with no exchange data. Residues whose amide protons did not exchange during the 46 h experiment were arbitrarily assigned a log P value of 7.

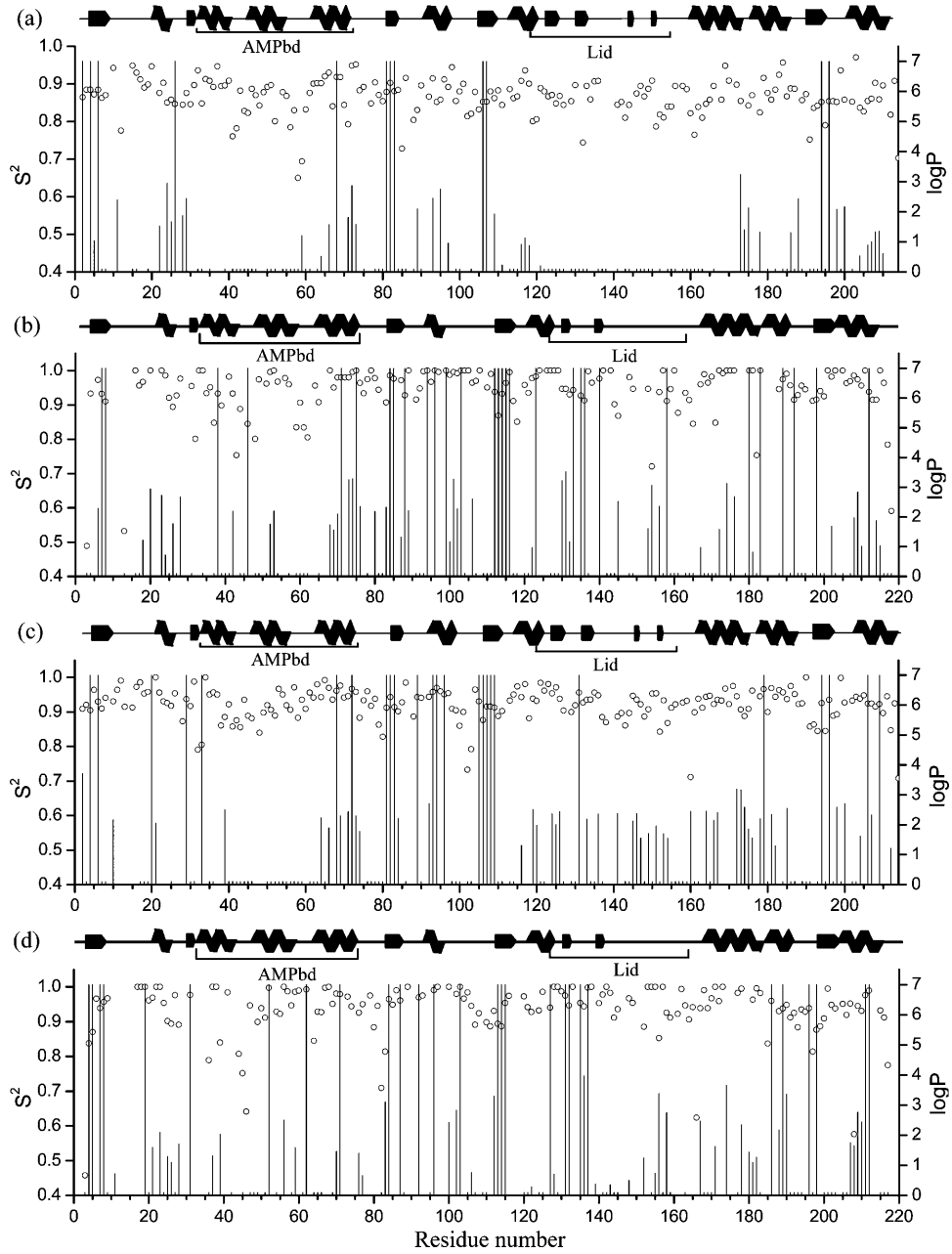

FIGURE 6: Sequence dependence of log of protection factors, P (■), in (a) ECAK, (b) TNAK, (c) ECAK*Ap5A, and (d) TNAK*Ap5A. S^2 values (○) for ECAK and ECAK*Ap5A (*33, 58*) and for TNAK and TNAK*Ap5A are shown. Residues that exchanged within the experimental dead time have been assigned an arbitrary log P of 0.1 to distinguish them from residues without any exchange data. Residues that did not exchange during the time course of the experiments have been assigned an arbitrary log P value of 7. Secondary structures and domains are indicated above the data.

Table 3: Percentages of Unprotected (UP), Moderately Protected (M), and Unexchanged (U) Amides in the Free and Inhibitor-Bound Forms of ECAK and TNAK[a]

	ECAK			TNAK			ECAK*Ap5A			TNAK*Ap5A		
protection	UP	M	U	UP	M	U	UP	M	U	UP	M	U
AMPbd	78.6	17.8	3.6	58.6	27.6	13.8	75	15.6	9.4	63.6	22.7	13.6
lid	96.4	3.6	0	53.8	26.9	19.2	48.4	48.4	3.2	39.1	39.1	21.7
core	40.9	42.4	16.6	42.5	30.1	27.4	43.5	27.5	29.0	38.5	32.3	29.2

[a] Percentages were calculated based on the number of residues in each domain that have exchange data.

The Slowest Exchanging Amide Hydrogens Are in the ECAK and TNAK Cores. Panels a and b of Figure 6 confirm that more amide protons in TNAK than in ECAK are unexchanged or have some level of protection from exchange. The domain distribution of protected amides in all four enzyme forms is summarized in Table 3. In ECAK, 59% of the core residues show some level of protection (i.e., M + U in Table 3), while only 21.4% and 3.6% of the AMPbd and lid residues, respectively, show any protection. This clear demarcation between a relatively rigid core and very flexible AMPbd and lid domains is absent in TNAK, where residues with moderate to high protection are distrib-

uted more uniformly throughout the protein (i.e., 57.5% in the core, 41.4% in the AMPbd domain, and 46.1% in the lid). Table 3 suggests that not all regions of the protein contribute to the higher stability of TNAK to the same extent. Indeed, the percentages of ECAK and TNAK core amides that show some protection level are very similar, indicating similar rigidity in the two enzyme cores. The rigidity increase occurs predominantly in TNAK's AMPbd and lid domains, which show approximately 2-fold (AMPbd) and 12-fold (lid) increases in the number of protected amide protons when compared to the corresponding ECAK domains (i.e., M + U in Table 3).

The slowest exchanging amide protons in native proteins are typically involved in well-ordered H-bond networks, or they are buried and have restricted solvent access. Exchange at these amides typically takes place only during global unfolding events. Although the percentages of protected amides are similar in the cores of ECAK and TNAK, the percentages of unexchanged amide protons suggest that TNAK's core is more rigid than ECAK's. Only 16.6% of ECAK's core amide protons are unexchanged compared to 27.4% in TNAK's core. Of the 12 ECAK amide protons that did not exchange during the time course of the experiment, 11 are located in the core domain. Of these 11 amide protons, 10 are in the β-strands, and 1 (Ile26) is in a loop. The only unexchanged amide proton not belonging to the core (Val68) is located in helix α4 of ECAK's AMPbd domain. Protection from exchange is usually associated with H-bonds. Even in the absence of H-bonds, though, residues can be protected by limiting solvent accessibility (*59, 60*). Using the ECAK crystal structure (PDB code 4ake), we computed the best possible H-bond network in the ECAK apo form (not shown) using the Optimal H-bonding Network module of the WHAT IF software (*61, 62*). WHAT IF results indicate that all of the unexchanged ECAK amide protons are involved in H-bonds. Particularly, the core amide protons form main chain H-bonds with other core residues, highlighting the importance of these interactions in the stability and rigidity of the core domain.

Of the 30 TNAK amide protons that did not exchange, 21 belong to core residues. In contrast to ECAK, though, while 13 of these unexchanged core amides belong to the core β-strands, as much as 8 of them belong to the core loops and α-helices, indicating a more rigid core domain in TNAK. Based on the WHAT IF analysis of our TNAK 3D model, each of these 21 core amide protons is involved in at least one H-bond with the main chain of another core residue. Some participate in additional H-bonds with side chains.

TNAK's lid is considerably more rigid than ECAK's, as indicated not only by the percentage of protected amides (M + U) but also by the number of unexchanged amides in this domain (five in TNAK's lid vs none in ECAK's lid.) TNAK's lid has four cysteines (Cys133, Cys136, Cys153, and Cys156) that bind a Zn^{2+} atom, forming a Zn-finger-like structure. Of the five unexchanged TNAK lid residues (Cys133, Lys135, Cys136, Tyr140, and Cys156), only the amides of Cys133, Tyr140, and Cys156 are involved in H-bonds according to our WHAT IF analysis. It is interesting to note that the amides of the corresponding ECAK residues are also involved in H-bonds, even though they are not protected. In ECAK, the TNAK Zn-finger-like structure is replaced by an H-bond network that may not be as stabilizing as the Zn finger. The structural role of Zn^{2+} as a stabilizing factor has been studied previously with a quadruple cysteine mutant ECAK (C4-ECAK) able to bind Zn^{2+}. Calorimetric studies showed that C4-ECAK is significantly more stable (its T_m increases from 51.8 to 63 °C) than the wild-type ECAK (*32, 63*). Correspondingly, removal of Zn^{2+} from TNAK reduces its T_m by nearly 6 °C (to 93.5 °C) (*31*). Thus, while Zn^{2+} is not the sole contributor to TNAK's thermostability, it plays an important role in stabilizing the lid. Zn^{2+} binding to the thiol groups of Cys133, Cys136, and Cys156 might contribute to stabilizing the lid H-bond networks. While the lid is, by far, the most flexible domain in ECAK, this domain appears slightly more rigid than the AMPbd domain in TNAK.

TNAK's AMPbd domain has four residues (Arg38, Asp46, Val71, and Leu75) in helices α2, α3, and α4 that have unexchanged amide protons. These amide protons are involved in similar H-bonds as the corresponding ECAK residues. In spite of this similarity, only the amide proton of ECAK Val68 remains unexchanged. Moderate to no protection is observed for the other three corresponding ECAK AMPbd amide protons (Arg36, Ser43, and Ile72).

Inhibitor-Binding Stabilizes ECAK's Core and Lid Domains and Destabilizes TNAK's AMPbd Domain. Panels c and d of Figure 6 show the plots of residue number vs log *P* values for ECAK*Ap5A and TNAK*Ap5A. Compared to ECAK, ECAK*Ap5A has 10% more residues that show protection against exchange (M + U in Table 3), a result consistent with ECAK's significant stabilization upon inhibitor binding. (ECAK*Ap5A's T_m is 10.5 °C higher than ECAK's.) A total of 25 residues in ECAK*Ap5A show no exchange during the time course of the experiment, against 12 in ECAK. The protection increase is not spread evenly among the different domains of the protein, though. While the percentages of protected amides are similar in the cores of ECAK (59%) and ECAK*Ap5A (56.5%), the percentage of unexchanged amide protons in ECAK*Ap5A's core almost doubles. All the unexchanged ECAK core amide protons remain protected in ECAK*Ap5A.

The most significant difference between ECAK and ECAK*Ap5A is in the lid. While all but one ECAK lid residue exchange during the dead time of the experiment, 51.6% of ECAK*Ap5A lid residues have some level of protection (M + U in Table 3). Only 3 of 16 partially protected amides have H-bonds that are absent in the free enzyme form. These observations suggest that additional H-bonds are not the only explanation for the significant protection against exchange detected in ECAK's lid upon inhibitor binding. Instead, enhanced protection of the lid residues could be due to a significant decrease in the lid's solvent-accessible surface area upon inhibitor binding.

In contrast to the lid, the AMPbd domain shows only marginal stabilization in ECAK*Ap5A, resulting in an AMPbd domain that is now less protected against exchange than the lid. Residues between 40 and 63 still exchange within the dead time of the experiment, indicating the high flexibility of this region in ECAK*Ap5A. The increase in the percentage of protected amides in the AMPbd domain is due to three unexchanged amide protons in helices α2 (Asp33) and α4 (Val68 and Arg71). It is interesting to note that none of these amides form H-bonds with Ap5A and that many of the intramolecular H-bonds they form are already

present in ECAK. Their protection in the inhibitor-bound form could result from an increase in the AMPbd domain rigidity that limits solvent accessibility.

In TNAK*Ap5A, the percentage of amide protons that show any protection from exchange increases only marginally compared to TNAK (~5%). This result is consistent with the fact that inhibitor binding does not increase TNAK's T_m. Many TNAK core residues remain unexchanged in TNAK*Ap5A as well, in agreement with the fact that many H-bonds are preserved in both conformational states. Even though fewer residues have exchange data in TNAK*Ap5A (127 residues) than in TNAK (150 residues), the protection distribution is highly similar in the cores of TNAK and TNAK*Ap5A. While the AMPbd domain seems somewhat destabilized in TNAK*Ap5A (M + U decreases by 5.1% in Table 3), the lid is the only domain that shows significantly increased protection upon inhibitor binding (M + U increases by 14.7%). Except for Cys136, the newly protected amides do not form any new intramolecular H-bonds (i.e., not found in TNAK), and they do not form H-bonds with Ap5A.

For both the AMPbd domain and the lid, the distribution of unexchanged amide protons is different in the two TNAK forms. For example, lid residue 158 remains unexchanged in TNAK, whereas it is only marginally stabilized in TNAK*Ap5A. Residue 137, which has no protection against exchange in TNAK, is fully protected in TNAK*Ap5A. Similarly, AMPbd domain residue 62 exchanges during the dead time of the experiment in TNAK, yet it is fully protected in TNAK*Ap5A. None of TNAK*Ap5A's unexchanged lid and AMPbd residues seem to form H-bonds with the inhibitor.

Hinge Regions. The AMPbd−core hinge regions consist of nine residues, of which five, six, eight, and four residues have exchange data in ECAK, TNAK, ECAK*Ap5A, and TNAK*Ap5A, respectively. The lid−core hinge regions consist of a total of 22 residues and 13, 15, 13, and 13 of these residues have exchange data in ECAK, TNAK, ECAK*Ap5A, and TNAK*Ap5A, respectively. As seen in Figure 6, amide protons from three of the five residues with exchange data in ECAK's AMPbd−core hinges and four of the six residues with exchange data in TNAK's AMPbd−core hinges have no protection from exchange. The remaining residues in both enzymes' AMPbd−core hinges have log *P* values below 3.0. In the lid−core hinges, the amide protons from 10 of 13 residues in ECAK and 11 of 16 residues in TNAK exchange within the dead time of the experiments. As was noted for the AMPbd−core hinges, amide protons of both enzymes' remaining lid−core hinge residues have log *P* values below 3.0. These results are not surprising since the hinge regions need to be highly flexible to allow large domain movements (*64*). In ECAK*Ap5A, 5 of 8 amide protons in the AMPbd−core hinges and 8 of 14 amide protons in the lid−core hinges have no protection from exchange. Corresponding numbers for TNAK*Ap5A are 1 of 4 in the AMPbd−core hinges and 8 of 13 in the lid−core hinges. In both ECAK*Ap5A and TNAK*Ap5A, interestingly, a single residue (Ile29 in ECAK*Ap5A and Ile31 in TNAK*Ap5A) in the AMPbd−core hinge remains unexchanged during the experiments. This Ile's amide forms an H-bond with an Asp (Asp84 in ECAK*Ap5A and Asp87 in TNAK*Ap5A) that is important for coordinating the catalytic Mg^{2+} (*65, 66*). A molecular dynamics simulation of ECAK in complex with MgATP and AMP shows that the H-bond between Asp84 and Ile29 is strong and stable (*67*), providing an explanation for the high protection of Ile29. At first sight Table 3 suggests that ECAK*Ap5A's AMPbd−core hinges contain a larger proportion of fast-exchanging residues than TNAK*Ap5A's AMPbd−core hinges. It is important to note, though, that we have exchange information for only 4 of the 9 hinge residues in TNAK*Ap5A. While we also have only partial exchange information for the lid−core hinges in ECAK*Ap5A and TNAK*Ap5A, two lines of evidence suggest that these hinges have very similar flexibility levels in the two enzymes: One, the same number of residues shows no protection or partial protection against exchange (Table 3). Second, the partially protected residues show comparable levels of protection, and their distribution along the hinge regions is very similar, as well.

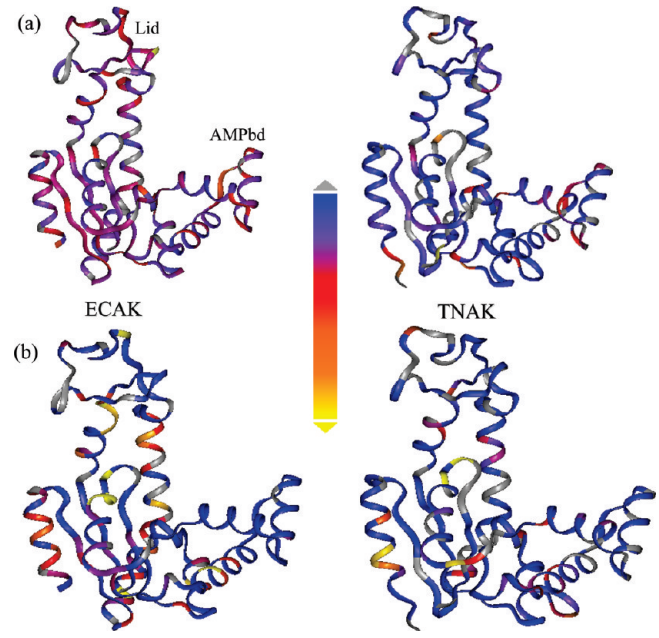

FIGURE 7: Backbone motions in ECAK and TNAK open forms. (a) Picosecond to nanosecond motions (S^2 values). (b) Microsecond to millisecond time scale dynamics. Color gradient goes from dark blue (rigid) to yellow (flexible). Residues with insufficient data are colored gray. ECAK data are from Shapiro et al. (*33*). The panels were generated using InsightII.

DISCUSSION

Over the past 2 decades much effort has been spent in investigating the relationships between flexibility, stability, and activity in hyperthermophilic enzymes. These investigations have been prompted by the fact that most hyperthermophilic enzymes are inactive at 30 °C. It is clear from these studies that the energy landscape of enzymes is complex, with motions that span picoseconds to minutes and that vary spatially. Comparison of TNAK's dynamics to those of ECAK and AAAK makes a unique case study to precisely investigate the relationship between flexibility, stability, and activity because of the unusually high activity of TNAK at 30 °C.

Fast (Picosecond to Millisecond) Time Scale Dynamics. It is clear from this study that TNAK is uniformly more rigid than ECAK at 30 °C in the picosecond to nanosecond time scale across all domains (Figure 7a). Increased S^2 values in TNAK, particularly in the core, indicate increased enthalpic

contribution to the thermodynamic stability of the native state (*15*), since the formation of enthalpically favorable interactions is expected to quench picosecond to nanosecond time scale motions. The rigidity of TNAK's core is further highlighted by the lack of microsecond time scale exchange in this region, unlike what is observed in ECAK's core [many more residues in ECAK's core, particularly in the β-strands, have R_{ex} values than in TNAK's core (Figure 7b)]. A similar observation was made for AAAK, which is also uniformly more rigid than ECAK at 20 °C (*9*). These results with TNAK and AAAK point to a strong link between picosecond to nanosecond time scale motions and stability. In contrast, the $\langle S^2 \rangle$ values of the three ECAK*Ap5A domains are similar to those of TNAK*Ap5A, indicating similar levels of rigidity on the picosecond to nanosecond time scale for both inhibitor-bound enzymes. Similar conclusions can be drawn from exchange contribution factors (R_{ex}) for dynamics on the microsecond to millisecond time scale: TNAK is more rigid than ECAK in the microsecond to millisecond time scale, but this rigidity difference almost disappears in the inhibitor-bound enzymes, because ECAK*Ap5A becomes substantially more rigid in that time scale. These results agree with our DSC findings that show that ECAK is significantly thermodynamically stabilized upon inhibitor binding but that TNAK is not.

Several TNAK residues, localized largely in the lid and AMPbd domain as well as in the hinges, are flexible, and they remain flexible in the closed form, TNAK*Ap5A. Additional hinge residues also become flexible specifically in the closed forms of ECAK and TNAK. Low $\langle S^2 \rangle$ values of the lid−core hinge loops in the inhibitor-bound forms conform to this trend. Our results agree with and further corroborate conclusions drawn from comparing AAAK and ECAK, where the authors find flexible hot spots located in the hinge regions. While these hot spots are rigid in AAAK at 20 °C, they become as flexible as in ECAK at 80 °C, consistent with AAAK's low activity at 20 °C. The hypothesis that these hinge residues contribute primarily to the motions required for activity appears to hold true (*9*). Although the role of picosecond to nanosecond time scale motions in slower catalytic processes is still not well understood, these high-frequency motions may ultimately facilitate the occurrence of slower motions for catalysis (*68*). Since $\langle S^2 \rangle$ values for all domains are higher in TNAK than ECAK, these flexible residues in key regions are located in the framework of a highly rigidified TNAK structure.

On the microsecond to millisecond time scale, analysis is complicated by the fact that R_{ex} values obtained by ^{15}N relaxation methods are not direct measurements of microsecond time scale motions and hence not reliable. ^{15}N relaxation dispersion experiments would be a better probe of motions on this time scale. Results presented here, though, point to trends that are consistent with TNAK's higher thermostability. More residues in ECAK have exchange contributions than in TNAK, and exchange contributions are largely absent in ECAK*Ap5A, in keeping with ECAK*Ap5A's increased rigidity seen in the picosecond to nanosecond time scale. These results are also consistent with the higher T_m of ECAK*Ap5A.

^{15}N relaxation dispersion experiments with thermophilic AAAK and mesophilic ECAK found that lid opening for product release was the rate-limiting step in the two enzymes (*24*). AAAK is 9 times less active than ECAK at 20 °C, and this lower catalytic activity is fully accounted for by AAAK's slower lid-opening rate measured at 20 °C. The fact that TNAK is highly active at 30 °C suggests that the higher picosecond to nanosecond time scale flexibility of the hinge regions together with the significant exchange contributions observed in TNAK*Ap5A's lid−core hinges reflect dynamics related to lid movements in catalysis. Since ^{15}N relaxation dispersion is a direct probe for microsecond time scale motions, it would be interesting to use this technique to measure lid-opening rates in TNAK and confirm this postulate.

Slower Time Scale Dynamics. To determine if trends in slow and fast dynamics coincide in ECAK and TNAK and to determine how they relate to TNAK's thermostability and activity properties, S^2 values are plotted along with log P values for ECAK, TNAK, ECAK*Ap5A, and TNAK*Ap5A in panels a, b, c, and d of Figure 6, respectively.

Comparing the ^{15}N relaxation dynamics and H−D exchange data for ECAK and TNAK shows some interesting differences in the two enzymes (Figure 6). $\langle S^2 \rangle$ values indicate only a marginally more rigid ECAK and TNAK core (relative to the rest of the protein) in the picosecond to nanosecond time scale (Table 1) and similar percentage increases in $\langle S^2 \rangle$ values of the core, lid, and AMPbd domains (8.5%, 9.5%, and 7.7%, respectively) going from ECAK to TNAK, suggesting a uniform rigidification across the entire hyperthermophilic enzyme in the picosecond to nanosecond time scale. On slower time scales, our H−D exchange results show that not only is TNAK not uniformly stabilized compared to ECAK, the two enzymes are not uniformly stabilized across all domains upon inhibitor binding (Figure 8). In the slow time scales, ECAK's core is significantly more rigid than the rest of the protein, with rigidity decreasing in the order core > AMPbd domain ≫ lid. TNAK shows a similar trend, with its core showing more protection from exchange than its other domains, although the difference between domains is not as marked as in ECAK.

As mentioned above, TNAK appears uniformly more rigid than ECAK at 30 °C in the picosecond to nanosecond time scale across all domains. In contrast, the H−D exchange data suggest that the AMPbd domain and the lid are considerably more rigid in TNAK than in ECAK in slower time scales but that the core is not. The only suggestion that TNAK's core is more rigid than ECAK's in our H−D exchange experiments resides in the fact that almost twice as many TNAK than ECAK core amides remain unexchanged during the 46 h experiment. Thus, unlike what was observed on the picosecond to nanosecond time scale, TNAK's increased rigidity on the millisecond and slower time scales is localized, rather than uniform, with most of the rigidification occurring in the lid, followed by the AMPbd domain.

Both the ^{15}N NMR relaxation and H−D exchange data show that ECAK's AMPbd domain is characterized by local fluctuations. Several residues in this domain have low S^2 values, and several feature model 5 type, subnanosecond to nanosecond time scale motions (*33*). The amide protons of ECAK residues 30 through 65 also exchange within the dead time of the experiments, indicating exchange through local fluctuations. Although TNAK's AMPbd domain is overall more rigid than ECAK's, it also has a number of residues showing low S^2 values (i.e., 32, 43, 46, 48, and 59−62),

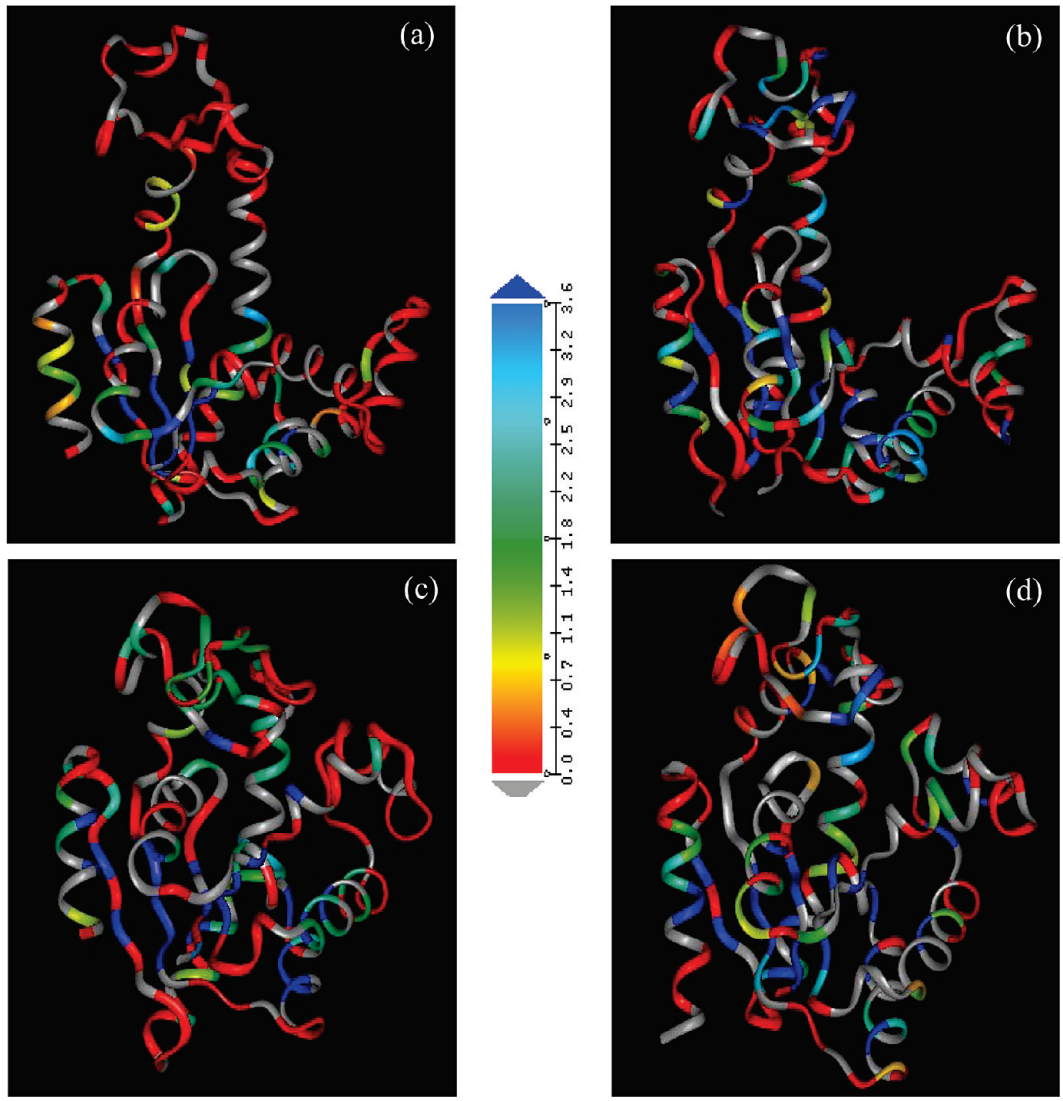

FIGURE 8: Protection factors summarized for (a) ECAK, (b) TNAK, (c) ECAK*Ap5A, and (d) TNAK*Ap5A backbones. Color gradient goes from blue (unexchanged residues) to red (residues that exchanged within the dead time of the experiments); gray indicates residues without exchange data. The panels were generated using InsightII.

with a similar S^2 value in both enzymes in many cases. Several amide protons between residues 33 and 65 in TNAK's AMPbd domain also are unprotected or show only moderate protection against exchange. Thus, both ECAK and TNAK's AMPbd domains feature dynamics in all the time scales studied here.

In contrast to the AMPbd domain, ECAK's lid does not show any significant trend in S^2 values. Several residues, though, show R_{ex} values indicating significant microsecond time scale dynamics. The lid is also the least protected from exchange in ECAK, indicating pervasive local fluctuations in the millisecond and slower time scales. Residues in TNAK's lid also show R_{ex} values, although these are fewer in number in TNAK than in ECAK. H−D exchange data show the TNAK lid to be more rigid than ECAK's (partly due to the presence of Zn^{2+}), although several residues in this region show only moderate protection. ECAK and TNAK's lids are thus characterized by motions mainly in time scales greater than microseconds.

Inhibitor binding brings up several dynamic changes of interest in the two enzymes. In the picosecond to nanosecond time scale, ECAK's three domains are stabilized to similar extents (5−8%) upon Ap5A binding, and they become almost as rigid as the corresponding domains in TNAK*Ap5A. In the millisecond and slower time scales, though, inihibitor binding stabilizes ECAK's lid to a much larger extent (with a 12-fold increase in the proportion of protected amides) than the core or the AMPbd domain. TNAK's lid is also significantly stabilized against exchange (M + U increases by 14.7%, Table 1) upon inhibitor binding, whereas it is unclear how significant the 4% increase (core) and the 5.1% decrease (AMPbd) in protected amides are. This large increase in protection against exchange for TNAK*Ap5A's lid suggests that the lid's $\langle S^2 \rangle$ increase from 0.935 to 0.96 (Table 1) is significant as well. In both inhibitor-bound enzymes, many AMPbd domain amide protons (24 in ECAK and 14 in TNAK) exchange within the dead time of the experiments, indicating considerable local fluctuations in this domain. In summary, upon inhibitor binding, the lid of both enzymes becomes significantly more rigid, the enzyme cores are only marginally stabilized, and TNAK's AMPbd domain becomes more prone to exchange (Figure 8c,d).

The loops belonging to the lid-core hinges of ECAK*Ap5A and TNAK*Ap5A show the same flexibility levels in the

picosecond to nanosecond time scale (they have almost identical, low $\langle S^2 \rangle$ values.) Two lines of evidence suggest that the same is true in the ms and slower time scales. First, the same numbers of residues show no protection or partial protection against exchange (Table 1). Second, the partially protected residues show comparable levels of protection, and these residues' distribution along the hinge regions is very similar, as well.

CONCLUSION

The results from this study show that TNAK, a multidomain protein in which catalysis-related motions mainly involve hinge movements, is simultaneously highly active at low temperatures and stable at high temperatures by localizing flexibility only to the hinge regions. The domains themselves are rigid without compromising activity at low temperatures, and localizing flexibility only to the hinges does not jeopardize the stability of the protein. These results suggest that proteins showing catalytic hinge movements or a catalytic site between well-defined, independent domains may be better templates than single-domain proteins for engineering both thermostability and high activity at low temperatures.

ACKNOWLEDGMENT

We thank Dr. Aizhou Liu for assistance with NMR data collection, Lishan Yao and Jake McKinlay for discussions, Maris Laivenieks for assistance with protein expression, and Dr. Charles Hoogstraten for critical reading of the manuscript. We also thank Dr. Martin Stone and Virginia Goehlert, Department of Chemistry, Indiana University, for the scripts to extract results from ModelFree output. Finally, we also thank Drs. Magnus Wolf-Watz and Dorothy Kern for providing us with AAAK's k_{cat} values.

SUPPORTING INFORMATION AVAILABLE

Figure S1, 600 MHz $^1H-^{15}N$ HSQC spectrum of TNAK at 30 °C, and Figure S2, 600 MHz $^1H-^{15}N$ HSQC spectrum of TNAK*Ap5A at 30 °C. This material is available free of charge via the Internet at http://pubs.acs.org.

REFERENCES

1. Vieille, C., and Zeikus, J. G. (2001) Hyperthermophilic enzymes: Sources, uses, and molecular mechanisms for thermostability. *Microbiol. Mol. Biol. Rev. 65*, 1–43.
2. Wrba, A., Schweiger, A., Schultes, V., Jaenicke, R., and Zavodsky, P. (1990) Extremely thermostable D-glyceraldehyde-3-phosphate dehydrogenase from the eubacterium *Thermotoga maritima*. *Biochemistry 29*, 7584–7592.
3. Zavodszky, P., Kardos, J., and Svingor, and Petsko, G. A. (1998) Adjustment of conformational flexibility is a key event in the thermal adaptation of proteins. *Proc. Natl. Acad. Sci. U.S.A. 95*, 7406–7411.
4. D'Amico, S., Marx, J. C., Gerday, C., and Feller, G. (2003) Activity-stability relationships in extremophilic enzymes. *J. Biol. Chem. 278*, 7891–7896.
5. Somero, G. N. (1978) Temperature adaptation of enzymes: Biological optimization through structure-function compromises. *Annu. Rev. Ecol. Syst. 9*, 1–29.
6. Gershenson, A., Schauerte, J. A., Giver, L., and Arnold, F. H. (2000) Tryptophan phosphorescence study of enzyme flexibility and unfolding in laboratory-evolved thermostable esterases. *Biochemistry 39*, 4658–4665.
7. Lazaridis, T., Lee, I., and Karplus, M. (1997) Dynamics and unfolding pathways of a hyperthermophilic and a mesophilic rubredoxin. *Protein Sci. 6*, 2589–2605.
8. Henzler-Wildman, K. A., Thai, V., Lei, M., Ott, M., Wolf-Watz, M., Fenn, T., Pozharski, E., Wilson, M. A., Petsko, G. A., Karplus, M., Hubner, C. G., and Kern, D. (2007) Intrinsic motions along an enzymatic reaction trajectory. *Nature 450*, 838–844.
9. Henzler-Wildman, K. A., Lei, M., Thai, V., Kerns, S. J., Karplus, M., and Kern, D. (2007) A hierarchy of timescales in protein dynamics is linked to enzyme catalysis. *Nature 450*, 913–916.
10. Hiller, R., Zhou, Z. H., Adams, M. W., and Englander, S. W. (1997) Stability and dynamics in a hyperthermophilic protein with melting temperature close to 200°C. *Proc. Natl. Acad. Sci. U.S.A. 94*, 11329–11332.
11. Manco, G., Giosue, E., D'Auria, S., Herman, P., Carrea, G., and Rossi, M. (2000) Cloning, overexpression, and properties of a new thermophilic and thermostable esterase with sequence similarity to hormone-sensitive lipase subfamily from the archaeon *Archaeoglobus fulgidus*. *Arch. Biochem. Biophys. 373*, 182–192.
12. Fitter, J., Herrmann, R., Dencher, N. A., Blume, A., and Hauss, T. (2001) Activity and stability of a thermostable α-amylase compared to its mesophilic homologue: Mechanisms of thermal adaptation. *Biochemistry 40*, 10723–10731.
13. Fitter, J., Herrmann, R., Dencher, N., and Blume, A. (2002) The role of protein dynamics for thermal adaptation of mesophilic and thermostable α-amylase. *Biophys. J. 82*, 304A–304A.
14. Hernandez, G., Jenney, F. E., Jr., Adams, M. W., and LeMaster, D. M. (2000) Millisecond time scale conformational flexibility in a hyperthermophile protein at ambient temperature. *Proc. Natl. Acad. Sci. U.S.A. 97*, 3166–3170.
15. Butterwick, J. A., Loria, J. P., Astrof, N. S., Kroenke, C. D., Cole, R., Rance, M., and Palmer, A. G. (2004) Multiple time scale backbone dynamics of homologous thermophilic and mesophilic ribonuclease HI enzymes. *J. Mol. Biol. 339*, 855–871.
16. Colombo, G., and Merz, K. M. (1999) Stability and activity of mesophilic subtilisin E and its thermophilic homolog: Insights from molecular dynamics simulations. *J. Am. Chem. Soc. 121*, 6895–6903.
17. Grottesi, A., Ceruso, M. A., Colosimo, A., and Di Nola, A. (2002) Molecular dynamics study of a hyperthermophilic and a mesophilic rubredoxin. *Proteins: Struct., Funct., Genet. 46*, 287–294.
18. Hollien, J., and Marqusee, S. (1999) Structural distribution of stability in a thermophilic enzyme. *Proc. Natl. Acad. Sci. U.S.A. 96*, 13674–13678.
19. Svingor, A., Kardos, J., Hajdu, I., Nemeth, A., and Zavodszky, P. (2001) A better enzyme to cope with cold—Comparative flexibility studies on psychrotrophic, mesophilic, and thermophilic IPMDHs. *J. Biol. Chem. 276*, 28121–28125.
20. Tsai, A. M., Udovic, T. J., and Neumann, D. A. (2001) The inverse relationship between protein dynamics and thermal stability. *Biophys. J. 81*, 2339–2343.
21. Fitter, J., and Heberle, J. (2000) Structural equilibrium fluctuations in mesophilic and thermophilic α-amylase. *Biophys. J. 79*, 1629–1636.
22. Grottesi, A., Ceruso, M. A., Colosimo, A., and Di Nola, A. (2002) Molecular dynamics study of a hyperthermophilic and a mesophilic rubredoxin. *Proteins 46*, 287–294.
23. Mandel, A. M., Akke, M., Arthur, G., and Palmer, I. (1995) Backbone dynamics of *Escherichia coli* ribonuclease HI: Correlations with structure and function in an active enzyme. *J. Mol. Biol. 246*, 144–163.
24. Wolf-Watz, M., Thai, V., Henzler-Wildman, K., Hadjipavlou, G., Eisenmesser, E. Z., and Kern, D. (2004) Linkage between dynamics and catalysis in a thermophilic-mesophilic enzyme pair. *Nat. Struct. Mol. Biol. 11*, 945–949.
25. Henzler-Wildman, K., and Kern, D. (2007) Dynamic personalities of proteins. *Nature 450*, 964–972.
26. Müller, C. W., and Schulz, G. E. (1992) Structure of the complex between adenylate kinase from *Escherichia coli* and the inhibitor Ap5A refined at 1.9 Å resolution—A model for a catalytic transition-state. *J. Mol. Biol. 224*, 159–177.
27. Müller, C. W., Schlauderer, G. J., Reinstein, J., and Schulz, G. E. (1996) Adenylate kinase motions during catalysis: An energetic counterweight balancing substrate binding. *Structure 4*, 147–156.
28. Schulz, G. E., Müller, C. W., and Diederichs, K. (1990) Induced-fit movements in adenylate kinases. *J. Mol. Biol. 213*, 627–630.
29. Gerstein, M., Schulz, G., and Chothia, C. (1993) Domain closure in adenylate kinase—Joints on either side of 2 helices close like neighboring fingers. *J. Mol. Biol. 229*, 494–501.

30. Gerstein, M., Lesk, A. M., and Chothia, C. (1994) Structural mechanisms for domain movements in proteins. *Biochemistry 33*, 6739–6749.
31. Vieille, C., Krishnamurthy, H., Hyun, H. H., Savchenko, A., Yan, H., and Zeikus, J. G. (2003) *Thermotoga neapolitana* adenylate kinase is highly active at 30°C. *Biochem. J. 372*, 577–585.
32. Perrier, V., Burlacu-Miron, S., Bourgeois, S., Surewicz, W. K., and Gilles, A. M. (1998) Genetically engineered zinc-chelating adenylate kinase from *Escherichia coli* with enhanced thermal stability. *J. Biol. Chem. 273*, 19097–19101.
33. Shapiro, Y. E., Sinev, M. A., Sineva, E. V., Tugarinov, V., and Meirovitch, E. (2000) Backbone dynamics of *Escherichia coli* adenylate kinase at the extreme stages of the catalytic cycle studied by ^{15}N NMR relaxation. *Biochemistry 39*, 6634–6644.
34. Sambrook, J., Fritsch, F. E., and Maniatis, T. (1989) *Molecular cloning: A laboratory manual*, Cold Spring Harbor Laboratory Press, Cold Spring Harbor, NY.
35. Reinstein, J., Brune, M., and Wittinghofer, A. (1988) Mutations in the nucleotide binding loop of adenylate kinase of *Escherichia coli*. *Biochemistry 27*, 4712–4720.
36. Grzesiek, S., and Bax, A. (1992) Correlating backbone amide and side-chain resonances in larger proteins by multiple relayed triple resonance NMR. *J. Am. Chem. Soc. 114*, 6291–6293.
37. Muhandiram, D. R., and Kay, L. E. (1994) Gradient-enhanced triple-resonance 3-dimensional NMR experiments with improved sensitivity. *J. Magn. Reson., B 103*, 203–216.
38. Yamazaki, T., Lee, W., Arrowsmith, C. H., Muhandiram, D. R., and Kay, L. E. (1994) A suite of triple-resonance NMR experiments for the backbone assignment of ^{15}N, ^{13}C, ^{2}H labeled proteins with high-sensitivity. *J. Am. Chem. Soc. 116*, 11655–11666.
39. Delaglio, F., Grzesiek, S., Vuister, G. W., Zhu, G., Pfeifer, J., and Bax, A. (1995) NMRPipe: a multidimensional spectral processing system based on UNIX pipes. *J. Biomol. NMR 6*, 277–293.
40. Johnson, B. A., and Blevins, R. A. (1994) NMRView: A computer program for the visualization and analysis of NMR data. *J. Biomol. NMR 4*, 603–614.
41. Kay, L. E., Keifer, P., and Saarinen, T. (1992) Pure absorption gradient enhanced heteronuclear single quantum correlation spectroscopy with improved sensitivity. *J. Am. Chem. Soc. 114*, 10663–10665.
42. Lipari, G., and Szabo, A. (1982) Model-free approach to the interpretation of nuclear magnetic-resonance relaxation in macromolecules. 1. Theory and range of validity. *J. Am. Chem. Soc. 104*, 4546–4559.
43. Lipari, G., and Szabo, A. (1982) Model-free approach to the interpretation of nuclear magnetic-resonance relaxation in macromolecules. 2. Analysis of experimental results. *J. Am. Chem. Soc. 104*, 4559–4570.
44. Clore, G. M., Driscoll, P. C., Wingfield, P. T., and Gronenborn, A. M. (1990) Analysis of the backbone dynamics of interleukin-1beta using two-dimensional inverse detected heteronuclear ^{15}N-proton NMR spectroscopy. *Biochemistry 29*, 7387–7401.
45. Clore, G. M., Szabo, A., Bax, A., Kay, L. E., Driscoll, P. C., and Gronenborn, A. M. (1990) Deviations from the simple two-parameter model-free approach to the interpretation of ^{15}N nuclear magnetic relaxation of proteins. *J. Am. Chem. Soc. 112*, 4989–4991.
46. Palmer, A. G., Rance, M., and Wright, P. E. (1991) Intramolecular motions of a zinc finger DNA-binding domain from Xfin characterized by proton-detected natural abundance ^{13}C heteronuclear NMR spectroscopy. *J. Am. Chem. Soc. 113*, 4371–4380.
47. Tugarinov, V., Shapiro, Y. E., Liang, Z., Freed, J. H., and Meirovitch, E. (2002) A novel view of domain flexibility in *E. coli* adenylate kinase based on structural mode-coupling ^{15}N NMR relaxation. *J. Mol. Biol. 315*, 155–170.
48. Garcia de la Torre, J. G., and VA, B. (1981) Hydrodynamic properties of complex, rigid, biological macromolecules: theory and applications. *Q. Rev. Biophys. 14*, 81–139.
49. Tjandra, N., Feller, S. E., Pastor, R. W., and Bax, A. (1995) Rotational diffusion anisotropy of human ubiquitin from ^{15}N NMR relaxation. *J. Am. Chem. Soc. 117*, 12562–12566.
50. Hiyama, Y., Niu, C. H., Silverton, J. V., Bavoso, A., and Torchia, D. A. (1988) Determination of ^{15}N chemical-shift tensor via ^{15}N-^{2}H dipolar coupling in boc-glycylglycyl [^{15}N] glycine benzyl ester. *J. Am. Chem. Soc. 110*, 2378–2383.
51. Bai, Y., Milne, J. S., Mayne, L., and Englander, S. W. (1993) Primary structure effects on peptide group hydrogen exchange. *Proteins 17*, 75–86.
52. Bai, Y. W., Englander, J. J., Mayne, L., Milne, J. S., and Englander, S. W. (1995) Thermodynamic parameters from hydrogen exchange measurements. *Methods Enzymol. 259*, 344–356.
53. Arrington, C. B., and Robertson, A. D. (2000) Kinetics and thermodynamics of conformational equilibria in native proteins by hydrogen exchange. *Methods Enzymol. 323*, 104–124.
54. Wildes, D., and Marqusee, S. (2004) Hydrogen-exchange strategies applied to energetics of intermediate processes in protein folding, in *Energetics of Biological Macromolecules, Part E*, pp 328−349.
55. Šali, A., and Blundell, T. L. (1993) Comparative protein modelling by satisfaction of spatial restraints. *J. Mol. Biol. 234*, 779–815.
56. Hayward, S. (2004) Identification of specific interactions that drive ligand-induced closure in five enzymes with classic domain movements. *J. Mol. Biol. 339*, 1001–1021.
57. Shapiro, Y. E., Kahana, E., Tugarinov, V., Liang, Z. C., Freed, J. H., and Meirovitch, E. (2002) Domain flexibility in ligand-free and inhibitor-bound *Escherichia coli* adenylate kinase based on a mode-coupling analysis of ^{15}N spin relaxation. *Biochemistry 41*, 6271–6281.
58. Shapiro, Y. E., Kahana, E., Tugarinov, V., Liang, Z. C., Freed, J. H., and Meirovitch, E. (2002) Domain flexibility in ligand-free and inhibitor-bound *Escherichia coli* adenylate kinase based on a mode-coupling analysis of ^{15}N spin relaxation. *Biochemistry 41*, 6271–6281.
59. Hilton, B. D., and Woodward, C. K. (1978) Nuclear magnetic resonance measurement of hydrogen exchange kinetics of single protons in basic pancreatic trypsin inhibitor. *Biochemistry 17*, 3325–3332.
60. Krishna, M. M., Lin, Y., Mayne, L., and Englander, S. W. (2003) Intimate view of a kinetic protein folding intermediate: residue-resolved structure, interactions, stability, folding and unfolding rates, homogeneity. *J. Mol. Biol. 334*, 501–513.
61. Hooft, R. W. W., Sander, C., and Vriend, G. (1996) Positioning hydrogen atoms by optimizing hydrogen-bond networks in protein structures. *Proteins: Struct., Funct., Genet. 26*, 363–376.
62. Rodriguez, R., Chinea, G., Lopez, N., Pons, T., and Vriend, G. (1998) Homology modeling, model and software evaluation: three related resources. *Bioinformatics 14*, 523–528.
63. Burlacu-Miron, S., Perrier, V., Gilles, A. M., Pistotnik, E., and Craescu, C. T. (1998) Structural and energetic factors of the increased thermal stability in a genetically engineered *Escherichia coli* adenylate kinase. *J. Biol. Chem. 273*, 19102–19107.
64. Sinev, M. A., Sineva, E. V., Ittah, V., and Haas, E. (1996) Domain closure in adenylate kinase. *Biochemistry 35*, 6425–6437.
65. Rose, T., Glaser, P., Surewicz, W. K., Mantsch, H. H., Reinstein, J., Le Blay, K., Gilles, A. M., and Barzu, O. (1991) Structural and functional consequences of amino acid substitutions in the second conserved loop of *Escherichia coli* adenylate kinase. *J. Biol. Chem. 266*, 23654–23659.
66. Yan, H. G., and Tsai, M. D. (1991) Mechanism of adenylate kinase. Demonstration of a functional relationship between aspartate 93 and Mg^{2+} by site-directed mutagenesis and proton, phosphorus-31, and magnesium-25 NMR. *Biochemistry 30*, 5539–5546.
67. Krishnamurthy, H., Lou, H. F., Kimple, A., Vieille, C., and Cukier, R. I. (2005) Associative mechanism for phosphoryl transfer: A molecular dynamics simulation of *Escherichia coli* adenylate kinase complexed with its substrates. *Proteins: Struct., Funct., Bioinf. 58*, 88–100.
68. Brooks, C. L., III, Karplus, M., and Pettitt, B. M. (1988) Proteins: A theoretical perspective of dynamics, structure, and thermodynamics, in *Advances in Chemical Physics* (Prigogine, I., and Rice, S. A., Eds.) John Wiley & Sons, New York.

BI802001W